

Elucidating the Impacts of COVID-19 Lockdown on Air Quality and Ozone Chemical Characteristics in India

Behrooz Roozitalab¹, Gregory R Carmichael¹, Sarath K Guttikunda², and Maryam Abdi-Oskouei³

¹University of Iowa

²Urban Emissions

³University Corporation for Atmospheric Research (UCAR)

November 28, 2022

Abstract

India implemented stay-at-home order (i.e. lockdown) on 24 March 2020 to decrease the spread of novel COVID-19, which reduced air pollutant emissions in different sectors. The Weather Research and Forecasting model with Chemistry (WRF-Chem) was used to study the changes in air pollutants during the lockdown period in 2020 compared with similar period in 2019. We found that both meteorology and lockdown emissions contributed to daytime PM_{2.5} (-6% and -11%, respectively) and ozone (-6% and -8%, respectively) reduction averaged in April 2020 in the Indo-Gangetic Plain. However, the ozone concentration response to reductions in its precursors (i.e. NO₂ and VOCs) due to the lockdown emissions was not constant over the domain. While ozone concentration decreased in most parts of the domain, it slightly increased in major cities like Delhi and in regions with many power plants. We utilized the reaction rates information in WRF-Chem to study the ozone chemistry. We found carbon monoxide, formaldehyde, isoprene, acetaldehyde, and ethylene as the major VOCs that contribute to the ozone formation in India. We used the ratio of chemical loss of radicals with radicals and NO_x, and its corresponding formaldehyde to NO₂ ratio (FNR) to find the ozone chemical regimes. Using the upper limit of FNR transition region (1.3), we found that most parts of India are within NO_x-limited regime while urban regions and the regions with many power plants are in a VOC-limited regime. As a result, policy makers should study the characteristics of a region before implementing mitigation strategies.

1 **Elucidating the Impacts of COVID-19 Lockdown on Air Quality and Ozone Chemical**
2 **Characteristics in India**

3 Behrooz Roozitalab^{1,2}, Gregory R. Carmichael^{1,2}, Sarath K. Guttikunda³, Maryam Abdi-Oskouei⁴

4 ¹Center for Global and Regional Environmental Research, University of Iowa, Iowa City, IA, USA

5 ²Chemical and Biochemical Engineering, University of Iowa, Iowa City, IA, USA

6 ³Urban Emissions, New Delhi, India

7 ⁴University Corporation for Atmospheric Research (UCAR), Boulder, CO, USA

8

9 Corresponding authors: B. Roozitalab (behrooz-roozitalab@uiowa.edu) and G. R. Carmichael
10 (gcarmich@engineering.uiowa.edu)

11

12 **Key Points:**

- 13 • Both emission and meteorological changes led to cleaner air during the lockdown period in April
14 2020 in India.
15 • Ozone formation in most parts of India is within NO_x-limited photochemical regime.
16 • Carbon monoxide, formaldehyde, isoprene, acetaldehyde, and ethylene are the major volatile organic
17 compounds of ozone formation in India.

18

19 **Abstract**

20 India implemented stay-at-home order (i.e. lockdown) on 24 March 2020 to decrease the spread of novel
21 COVID-19, which reduced air pollutant emissions in different sectors. The Weather Research and
22 Forecasting model with Chemistry (WRF-Chem) was used to study the changes in air pollutants during
23 the lockdown period in 2020 compared with similar period in 2019. We found that both meteorology and
24 lockdown emissions contributed to daytime $PM_{2.5}$ (-6% and -11%, respectively) and ozone (-6% and -8%,
25 respectively) reduction averaged in April 2020 in the Indo-Gangetic Plain. However, the ozone
26 concentration response to reductions in its precursors (i.e. NO_2 and VOCs) due to the lockdown emissions
27 was not constant over the domain. While ozone concentration decreased in most parts of the domain, it
28 slightly increased in major cities like Delhi and in regions with many power plants. We utilized the
29 reaction rates information in WRF-Chem to study the ozone chemistry. We found carbon monoxide,
30 formaldehyde, isoprene, acetaldehyde, and ethylene as the major VOCs that contribute to the ozone
31 formation in India. We used the ratio of chemical loss of radicals with radicals and NO_x , and its
32 corresponding formaldehyde to NO_2 ratio (FNR) to find the ozone chemical regimes. Using the upper
33 limit of FNR transition region (1.3), we found that most parts of India are within NO_x -limited regime
34 while urban regions and the regions with many power plants are in a VOC-limited regime. As a result,
35 policy makers should study the characteristics of a region before implementing mitigation strategies.

36 **1. Introduction**

37 While COVID-19 virus is a global disaster in terms of its health and economy damages, it provides a
38 unique opportunity in earth system sciences (Gorris et al., 2021). As many countries initiated stay-at-
39 home orders (hereafter called lockdown) in early 2020 to control the spread of the virus, anthropogenic
40 air pollutant emissions started to decline in different sectors (Doubmbia et al., 2021). While many studies
41 had used numerical models to understand the impacts of stringent future emission control “scenarios” on
42 air quality (Amann et al., 2020), worldwide lockdowns introduced a scenario accompanied by actual
43 observational data. As a result, numerous studies have studied the changes in air pollution using ground
44 measurements (e.g. Shi and Brasseur (2020)) and satellite data (e.g. Goldberg et al. (2020)). An
45 exhaustive review on these studies can be found in Gkatzelis et al. (2021). However, these data have
46 spatial or/and temporal gaps. In order to utilize the models, some studies used available activity data (e.g.
47 Doubmbia et al. (2021)) or inverse modeling (e.g. Souri et al. (2021)) to update emission inventories.

48 Air pollution is a concerning issue in India due to its large health and environmental impacts (Ghude et
49 al., 2014; HEI, 2018). While even extreme air pollution events are not unusual in India (Roozitalab et al.,
50 2021), clean air due to the lockdown was unusual and attracted people and media’s attention (Gupta,
51 2020). In India, the lockdown officially started on 24 March 2020 and continued in four phases until the
52 end of May 2020. While residential and power sectors emissions did not show large changes, large
53 emission reductions were reported in other sectors such as transportation (Beig et al., 2021). This
54 reduction in emissions resulted in different changes in air quality over India. Relatively short lifetime of
55 NO_2 makes it a suitable tracer of local NO_x emissions (Goldberg et al., 2019). Figure 1 shows the
56 tropospheric column NO_2 concentration in April 2019 and 2020 over northern India retrieved from the
57 TROPospheric Monitoring Instrument (TROPOMI) satellite data. Lower values in April 2020 compared
58 with 2019 indicate reductions in NO_x emissions in most parts of India except the thermal power plant
59 regions. For example, NO_2 concentrations showed large reductions over Delhi and other urban regions
60 due to the lower activities in transportation sector. However, the demand for electricity showed small
61 changes during the lockdown period; NO_2 concentrations did not change very much over the thermal

62 power plants region (ESA, 2020). Other studies using TROPOMI and Ozone Monitoring Instrument
63 (OMI) satellites and ground measurements data confirmed these changes (Biswal et al., 2020).

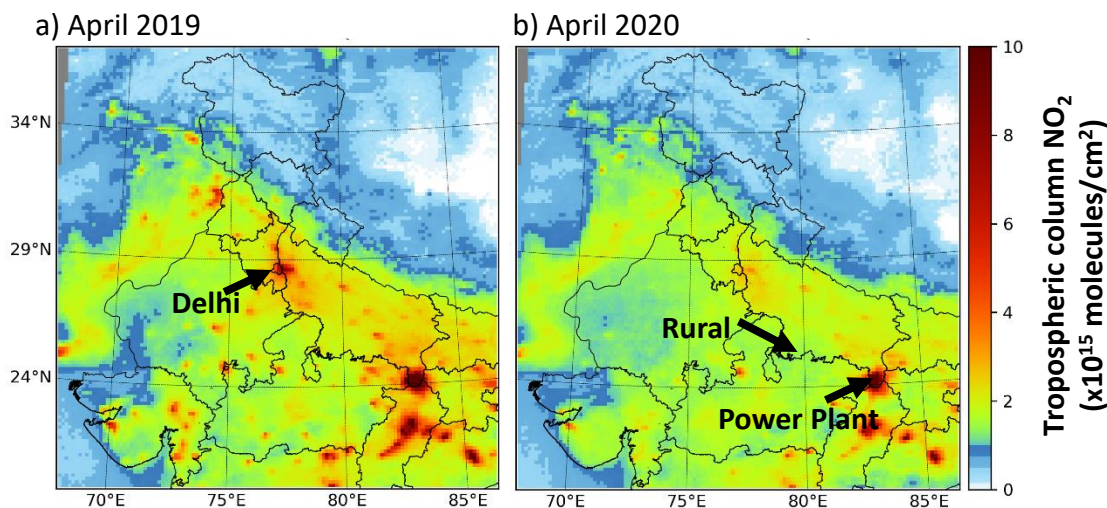
64 Many studies used measurement data and studied the changes in air pollutant concentrations in Indian
65 regions during different phases of the lockdown period (Jain & Sharma, 2020; V. Kumar et al., 2020;
66 Kumari & Toshniwal, 2020; Mahato et al., 2020; Selvam et al., 2020; Singh et al., 2020). While the
67 studied periods are different in each study, the conclusion was solid. All of them found significant
68 reductions in PM_{2.5} and NO₂ concentrations when compared to pre-lockdown period or previous years. A
69 limited number of studies have also investigated the lockdown emission effects in India. Zhang et al.
70 (2021) used WRF-CMAQ model to study the pre-lockdown-to-lockdown air quality changes in India,
71 between 21 February and 24 April 2020, by decreasing the emissions in industrial (82%), transportation
72 (85%), and energy (26%) sectors during the lockdown period. They found that air quality improved over
73 India for all the pollutants with some exceptions of MDA8 ozone for some urban areas. Dumka et al.
74 (2021) used the WRF-CHIMMERE model and simulated significantly lower PM_{2.5} and NO₂
75 concentrations over India during the lockdown period (25 March and 17 May 2020) compared with the
76 pre-lockdown period by completely excluding traffic and industrial sectors from the emission inventory.
77 Gaubert et al. (2020) used CESM2 model and adjusted emission based on the work by Doumbia et al.
78 (2021) to study the meteorological and lockdown emission impacts on the secondary atmospheric
79 pollutants during the lockdown period over the world. They found that the lockdown emissions reduced
80 ozone in India, while meteorology had both decreasing and increasing effect on ozone concentration. In
81 general, the above-mentioned studies found unexpected changes in ozone concentrations. While large
82 reductions in NO₂ concentration, as its' precursor, were found, lower reductions were reported in ozone
83 concentrations (Zhang et al., 2021). Moreover, some enhancements in observed ozone concentrations
84 compared with the pre-lockdown period were found (Kumari & Toshniwal, 2020; Mor et al., 2021).
85 Similarly in global scale, Miyazaki et al. (2020) found that NO_x emission reductions due to the COVID-
86 19 lockdowns led to about 2% reduction in the global tropospheric ozone burden, while surface ozone
87 concentrations increased in some regions (Shi & Brasseur, 2020; Sicard et al., 2020).

88 Different response of ozone to its precursors' changes is due to its complicated chemistry. Chen et al.
89 (2020) studied the sensitivity of ozone formation to its precursors and aerosol loading in Delhi. They
90 found that a reduction by more than 65-80% in NO_x emissions alone was needed to reduce the ozone
91 concentration, whereas VOC emission reductions were the efficient control strategy. On the other hand,
92 the effects of meteorology should also be considered when studying the differences in concentrations
93 between 2020 and previous years. Gkatzelis et al. (2021) found only about one-third of all the global
94 studies on the effects of COVID-19 accounted for impacts of changing meteorology. For example,
95 Goldberg et al. (2020) showed that meteorological conditions alone decreased tropospheric column NO₂
96 concentration by a median of 21.6% in the United States (US) in 2020 compared with 2019. Different
97 meteorology can also change the amounts of biogenic emissions, dust emissions, and biomass burning
98 emissions. As a result, a modeling study is required to investigate the impacts of meteorology and
99 lockdown emissions on the air quality during the lockdown period. Furthermore, numerous modeling
100 studies have been performed over India with the primary focus on PM (Garaga et al., 2018), while only a
101 few of them have studied ozone (Luke Conibear et al., 2018; Ghude et al., 2016; Kota et al., 2018; R.
102 Kumar et al., 2012; Sharma et al., 2017).

103 The objectives of this study are to understand 1) how the meteorology and COVID-19 lockdown
104 emissions affected air quality in northern India and 2) how ozone precursor's emissions contributed to
105 ozone formation in India. To achieve these objectives, we used the regional Weather Research and
106 Forecasting Model with Chemistry (WRF-Chem) version 4 to simulate the air quality during March and

107 April in 2019 and 2020. We also utilized the Integrated Reaction Rate (IRR) capability in this version to
108 understand how ozone formed in different regions (i.e. urban, non-urban, and a thermal power plant
109 region) in India and how it changed during the lockdown period. To account for emission changes during
110 the COVID-19 lockdown period, we used the adjustment factors proposed by Doumbia et al. (2021).

111 The paper is organized as follows. First, we provide a description of the WRF-Chem model and
112 adjustment factors used to account for the lockdown period emissions, and evaluate the modeling results
113 against ground measurements data in 2019 and 2020. Then, we study the effects of meteorology and
114 lockdown emissions on air quality using different modeling experiments. Finally, we use the IRR and
115 study the ozone chemistry in different regions in India and provide a summary of the findings.



116
117 Figure 1 Tropospheric column NO₂ concentrations over the WRF-Chem modeling domain averaged for April a) 2019 and b)
118 2020 retrieved from TROPOMI on board the Copernicus Sentinel-5 Precursor satellite. The three regions used for process
119 analysis has been marked and also shown on Figure S1. The quality assurance more than 0.5 was used.

120 2. Methods:

121 2.1. WRF-Chem modeling

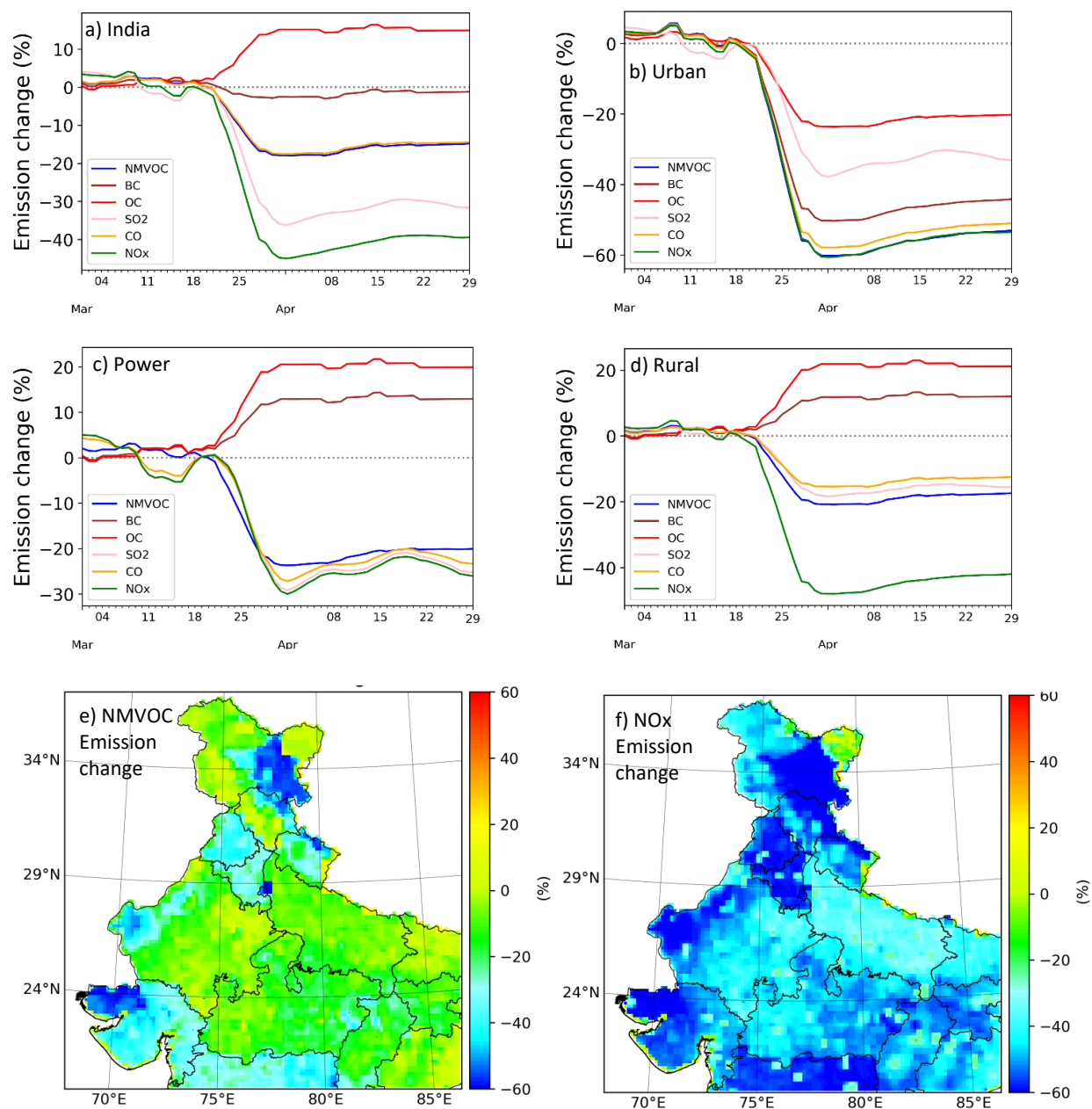
122 WRF-Chem model version 4.0 was used in this study in order to utilize its new IRR capability (Grell et
123 al., 2005; Pfister et al., 2019). We used a single domain, centered over Delhi, which covered the Indo-
124 Gangetic Plain (IGP) and central India with a 15 km x 15 km resolution and 39 vertical layers (Figure 1;
125 location of the IGP is shown in Figure S6). The Model for Ozone and Related chemical Tracers, version 4
126 (MOZART-4) introduced by Emmons et al. (2010) with updates on monoterpenes (Hodzic et al., 2015)
127 and isoprene oxidations (Knote et al., 2014) was selected as the gas phase chemistry mechanism (More
128 information on the evolution of the MOZART mechanism can be found in Emmons et al. (2020)). For
129 aerosol representation, the four-bin MOdel for Simulations Aerosol Interactions and Chemistry
130 (MOSAIC-4bin) introduced by Zaveri et al. (2008) with updates for Secondary Organic Aerosol (SOA)
131 formation (Hodzic & Jimenez, 2011) was selected.

132 Initial and boundary condition (IC/BC) for meteorological fields were provided by National Center for
133 Atmospheric Prediction Global Forecasting System Final Analysis (NCEP GFS-FNL) data
134 (<https://rda.ucar.edu/datasets/ds083.2/>, last access: 20 December 2020). For Chemical IC/BC, we used the

135 Whole Atmosphere Community Climate Model (WACCM) outputs (*Whole Atmosphere Community*
136 *Climate Model (WACCM) Model Output*, 2020). We reinitialized the model every 30-hours and updated
137 meteorological IC/BC and chemical boundary conditions but used the chemical initial condition from the
138 previous cycle. The re-initialization for every cycle started during nighttime at 1800 UTC (2330 Local
139 Time (LT)) and the first 6 hours were discarded as spin up following Abdi-Oskouei et al. (2018). The
140 simulation period included March and April in 2019 and 2020, while we primarily focus on April results.
141 The details of other configuration options can be found in Roozitalab et al. (2021).

142 We used the Hemispheric Transport of Air Pollution emission inventory (HTAP v2.2) 0.1x0.1 degree
143 gridded monthly-averaged for each sector as our base anthropogenic emission inventory (Janssens-
144 Maenhout et al., 2015). The speciation provided by Emissions of atmospheric Compounds and
145 Compilation of Ancillary Data (ECCAD) database for Non Methane Volatile Organic Carbons
146 (NMVOCs; hereafter NMVOCs refer to VOCs except Methane and CO and VOCs refer to their
147 inclusion), which is based on ratios in the RETRO project (<https://permalink.aeris-data.fr/HTAPv2>, last
148 access: 20 December 2020). Moreover, the mapping between the ECCAD NMVOCs and model emitted
149 species are provided in Table S1 (personal communications with Louisa Emmons, NCAR). In this study,
150 we arbitrarily chose three regions representing an urban, a rural, and a power plant region when analyzing
151 the ozone chemistry (Figure 1). The urban region contains the greater Delhi region (hereafter called
152 Urban), the rural area contains a non-urban region with low population density in the border of Uttar
153 Pradesh and Madhya Pradesh states (hereafter called Rural), and the power plant region covers an area
154 with high emission thermal power plants (hereafter called Power). To keep the regions comparable with
155 each other, each region includes a set of 4x5 grid cells in the model (~4500 km²; Figure S1). Hereafter,
156 we also call the Indian regions of the domain as India. The amount of HTAP v2.2 emissions for different
157 species over these defined regions for the month of March and April are shown in the supporting
158 information (Table S2 and Table S3). Urban had the highest emissions for all the species except for SO₂.
159 SO₂ emissions were higher in Power. The amount of NO_x emission was close in Urban and Power
160 regions. On the other hand, NMVOC emissions were very low in Power and Rural. Emissions in April
161 were lower than March for all the regions; however, this difference was very small for Rural as the
162 emissions were originally low.

163 To consider emission reductions due to the lockdown in 2020, we used the adjustment factors (AFs)
164 provided by Doumbia et al. (2021). Doumbia et al. (2021) estimated the global gridded AFs based on the
165 change of activity data for each sector with respect to a five-week period starting on January 2020. Figure
166 2 shows the daily change of emissions for a) India, b) Urban, c) Power, and d) Rural. It shows a small
167 fluctuation in emissions until 24 March (as adjusting factors are with regard to January), with a dramatic
168 change afterwards due to initiation of the lockdown. The lockdown had the largest impact on NO_x
169 emission with greater than 40% reduction averaged over India. The emissions of SO₂ also showed large
170 reductions with smaller reductions for NMVOCs and CO. Black carbon did not change very much over
171 India, while Organic Carbon (OC) increased after the lockdown due to increased fuel consumption for
172 residential sector (Yadav et al., 2020). The total changes in emission in each region depends on both the
173 AFs and the amount of emission from each sector in that region. Urban showed similar emission
174 reductions for both NO_x and NMVOCs as for India. Reduction in emission of NMVOC was lower than
175 NO_x in Power and Rural. Moreover, the amount of emission change was different as well. For example,
176 NO_x emissions reduced by up to 60%, 50%, and 30% in Urban, Rural, and Power, respectively. On the
177 other hand, OC and black carbon decreased in Urban, while increased over other regions. Figure 2 (e, f)
178 also shows the maps of averaged emission reductions in April 2020 for NMVOC and NO_x. Although
179 these results are qualitatively consistent with results in Gaubert et al. (2020), there are some quantitative
180 differences, primarily due to different base emission inventory and considered regions.



181
 182 Figure 2 Daily Emission change due to AF applied on HTAP v2.2 emissions averaged in a) India, b) Urban, c) Power, and d)
 183 Rural (X-axis shows the days in March and April and Y-axis range is different for each subplot). Map of emission changes of e)
 184 NMVOC and f) NOx averaged in April 2020.

185 The Fire Inventory from NCAR, version 2.2 (FINN v2.2) based on MODIS fire detections was used as
 186 the biomass burning emission inventory (Wiedinmyer et al., 2011). Comparing the fire emissions between
 187 2019 and 2020 during the studied period showed lower total emissions in 2020 (Figure S2), with most of
 188 the fires over central parts of the domain. However, it also showed that some days in 2020 (e.g. 16 April)
 189 had much larger emissions compared with 2019. We also used the online Model of Emissions of Gases
 190 and Aerosols from Nature (MEGAN v. 2.0.4) as the biogenic emission inventory (Guenther et al., 2006).
 191 MEGAN emissions changed between years 2019 and 2020 as they are based on meteorological fields (i.e.

192 temperature). For Dust emissions, we used the online Goddard Global Ozone Chemistry Aerosol
 193 Radiation and Transport (GOCART) mechanism.

194 To study the response of air quality to both meteorological and emission forcings, we performed four
 195 simulations (Table 1). It should be noted the we considered all emission sources that are directly (i.e.
 196 biogenic and wind-blown dust) and indirectly (biomass burning) related to the meteorology as
 197 meteorological forcings. The reason is that the lockdown anthropogenic emissions' adjustments do not
 198 directly affect these sources. In the 2019BAU scenario, all the year-dependent input data including
 199 chemical and meteorological IC/BC, and biomass burning emissions were from 2019. As a result, online
 200 biogenic and dust emissions also followed 2019 meteorology. Moreover, we used HTAP v2.2 emission
 201 inventory as Business As Usual (BAU) anthropogenic emission in 2019BAU. Following the same logic,
 202 2019COVID means 2019 year-dependent input data, while anthropogenic emissions were adjusted based
 203 on the multiplication of HTAP v2.2 and AFs for each sector. Similarly, 2020BAU was based on 2020
 204 year-dependent input data and BAU anthropogenic emission, while 2020COVID used adjusted emissions.
 205 These four scenarios provide an opportunity to look at the effects of meteorology, emissions, and their
 206 combined effects on air quality over the domain.

207 Table 1 List of scenarios performed in this study

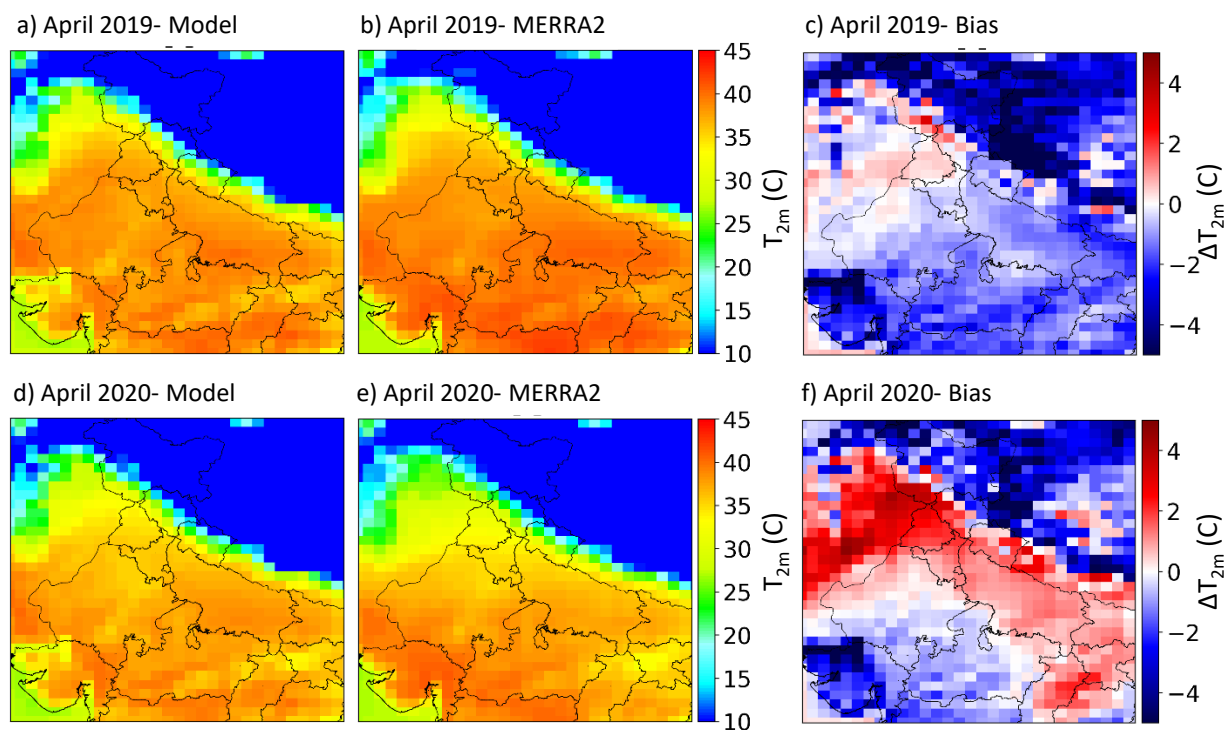
Scenario	Meteorology	Anth. Emission	Biomass Burning Emission	Biogenic Emission	Dust Emission	Initial/Boundary Condition
2019BAU	2019	HTAP v2.2	2019	2019	2019	2019
2019COVID	2019	HTAP v2.2 adjusted with AF	2019	2019	2019	2019
2020BAU	2020	HTAP v2.2	2020	2020	2020	2020
2020COVID	2020	HTAP v2.2 adjusted with AF	2020	2020	2020	2020

208

209 2.2. Model evaluation

210 We evaluated the performance of the model compared with ground measurements and global reanalysis
 211 data. Scenarios 2019BAU and 2020COVID should represent the real states of the atmosphere for years
 212 2019 and 2020, respectively. In the following model evaluation discussion, the model for 2019 refers to
 213 2019BAU and the model for 2020 refers to 2020COVID results. For meteorological fields, we compared
 214 the model with the Modern-Era Retrospective analysis for Research and Applications, Version 2
 215 (MERRA-2) data (Bosilovich et al., 2015). Hourly statistics for a location in Delhi (28.6 N, 77.19 E)
 216 showed 2-m temperature (T_{2m}) mean error (ME) of 2.9 °C and 3.5°C in 2019 and 2020, respectively, and
 217 10-m wind speed (WS_{10m}) of 1.3 m/s and 1.3 m/s in 2019 and 2020, respectively. The root mean squared
 218 error (RMSE) for T_{2m} was 3.4 °C and 4.1 °C in 2019 and 2020, respectively. The RMSE for WS_{10m} was
 219 1.7 m/s and 1.6 m/s for 2019 and 2020, respectively. These are comparable with Zhang et al. (2021)
 220 values when modeling the pre-lockdown and lockdown period in India. The model satisfied the wind
 221 speed ME goal of 2.0 m/s, while overestimated temperature ME goal of 2.0 °C, proposed by Emery et al.
 222 (2001). The model simulated the daytime (1000-1700 LT) T_{2m} peaks but overestimated nighttime values
 223 (Figure S3). Figure 3 shows the averaged hourly T_{2m} over the domain for April 2019 and 2020 in the
 224 model (re-gridded to MERRA-2 resolution) and MERRA-2. The model captured the general spatial

225 pattern of temperature in both 2019 and 2020. However, the model was biased low over most parts of
 226 India in 2019. On the other hand, the model was biased high over the IGP and biased low over central
 227 India in 2020. It also shows that the model was biased high over the western parts of the IGP in both 2019
 228 and 2020. Comparing WS_{10m} also indicated the ability of the model to capture the spatial pattern, while
 229 the model was biased low most of the time in Delhi (Figure S4). The differences in the meteorology can
 230 affect the air quality by changing the natural emission sources (e.g. dust and biogenic emissions).
 231 Furthermore, the dynamics of the atmosphere (e.g. boundary layer height and wind) change how the air
 232 pollutants disperse and transport in the atmosphere.



233
 234 Figure 3 Averaged hourly 2-m temperature in April 2019 (top row) and 2020 (bottom row) in the WRF-Chem model (left
 235 column), MERRA-2 (middle column), and their difference (right column).

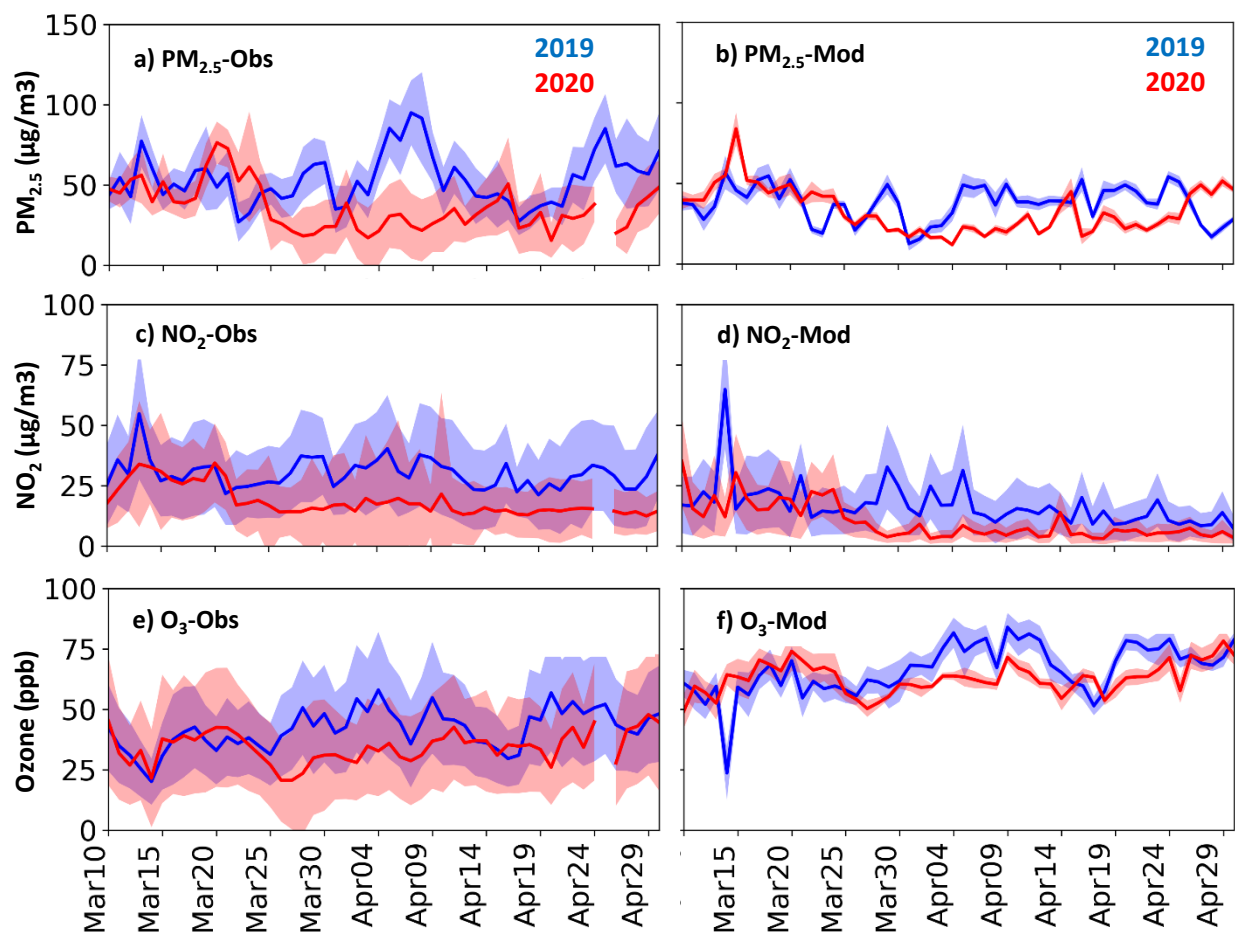
236 We used the hourly ground measurements air pollutant concentrations data in Delhi collected by the
 237 Central Pollution Control Board (CPCB) to evaluate the air quality in years 2019 and 2020. Other than
 238 the original quality control filters applied by the CPCB ([https://cpcb.nic.in/quality-assurance-quality-](https://cpcb.nic.in/quality-assurance-quality-control/)
 239 [control/](https://cpcb.nic.in/quality-assurance-quality-control/), last access: 02/23/2021), we applied four additional filters (Jena et al., 2020; Singh et al., 2020).
 240 First, we removed the stations with all zero or not-a-number (i.e. NAN) values. Second, we removed the
 241 stations with no variation, in which the standard deviation (STD) of the data was less than five percent of
 242 its mean. Third and fourth, we removed the outlier values, in which the difference between two
 243 consecutive hours was more than 100 units (except for carbon monoxide (CO), for which we used a cut-
 244 off of 300 $\mu\text{g}/\text{m}^3$) or the difference between each value and the mean value was higher or lower than
 245 $3 \times \text{STD}$.

246 The model evaluation statistics for $\text{PM}_{2.5}$, ozone, NO_2 , and CO during April 2019 and 2020 were
 247 calculated for daytime (1000-1700 LT) and 24-hour average (i.e. daily) period and are provided in the
 248 supporting information (Table S4 and Table S5). The normalized mean bias (NMB) for daily $\text{PM}_{2.5}$ was -
 249 31% and -17% in April 2019 and April 2020, respectively. Zhang et al. (2021) simulated the period

250 between 21 February and 23 March in 2020 and reported PM_{2.5} mean normalized bias (MNB) of -16% in
251 Delhi. Roozitalab et al. (2021) reported NMB of -17% in their best experiment for modeling PM_{2.5} in an
252 extreme pollution event in November 2017. The model overestimated daytime ozone concentrations with
253 NMB of 43% and 78% in April 2019 and April 2020, respectively. On the contrary, the model was biased
254 low for NO₂ by daytime NMB of -35% and -47% for April 2019 and April 2020, respectively. The model
255 underestimated daytime CO concentrations by NMB of -67% and -64% for April 2019 and April 2020,
256 respectively. Kota et al. (2018) modeled air quality in India in 2015 and reported NMB of 53%, -33%,
257 and -54% for ozone, NO₂, and CO, respectively, in Delhi. Other studies have also reported overestimation
258 of simulated ozone concentrations over Delhi (Luke Conibear, 2018; Ghude et al., 2016; R. Kumar et al.,
259 2012; Pommier et al., 2018). On the contrary, Sharma et al. (2017) underestimated diurnal ozone by 16
260 ppb in Delhi. Furthermore, Zhang et al. (2021) slightly underestimated ozone in Delhi by MNB of -4%.
261 They also reported MNB of -51% and -59% for NO₂ and CO, respectively. Overall, the model
262 performance for PM_{2.5} was similar to other studies and daily NMB is within the benchmark criteria of
263 Emery et al. (2017). However, the model was biased low for daytime ozone precursors (NO₂ and CO)
264 concentrations and biased high for daytime ozone mixing ratios.

265 We explored the extent to which model performance was influenced by the year the emission inventory
266 was based on. The HTAP v2.2 emissions used in these simulations are estimates for 2010. As a result, we
267 performed a set of experiments using the Copernicus Atmosphere Monitoring Service global emission
268 inventory version 4.2 (CAMS v4.2; Granier et al. (2019)). Our analysis indicated that the concentrations
269 and changes in concentrations due to lockdown emissions were close in both CAMS and HTAP emissions
270 (More information can be found in supporting information). As a result, we performed all further analysis
271 in this study based on HTAP anthropogenic emission inventory. Figure 4 shows the averaged daytime
272 PM_{2.5}, NO₂, and ozone concentrations measured (left panels) and modeled (right panels) between 10
273 March and 30 April in 2019 (blue colors) and 2020 (red colors) in Delhi. Both measured data and the
274 model showed similar values in 2019 and 2020 between 10 March and around 24 March (before
275 lockdown) accompanied by a drop afterwards (during lockdown). However, the day that concentrations
276 dropped is different between the measured data (22 March) and the model (24 March). Yadav et al.
277 (2020) also reported that the lockdown was not abrupt and had a transition start. Furthermore, the
278 averaged amount that concentrations dropped during the lockdown period (24 March-30 April) in 2020
279 compared with 2019 was different between measured data and the model. Mean reduction for daytime
280 PM_{2.5} concentrations was 26 µg/m³ in measured data, while the model showed a smaller drop (9 µg/m³).
281 For daytime NO₂, the measured data decreased by 14 µg/m³ (50%), while the modeled outputs decreased
282 by 8 µg/m³ (61%). Vadrevu et al. (2020) also reported 61% reduction in TROPOMI tropospheric column
283 NO₂ concentrations during 25 March and 3 May in 2020 compared with 2019. Daytime ozone mixing
284 ratio also dropped during the lockdown in both measured (10 ppb) and modeled (7 ppb) data. However,
285 24-hour averaged ozone mixing ratio did not change very much neither in the measured data nor in the
286 model although small fluctuations were observed between years 2019 and 2020 (Figure S5). We will
287 further analyze this behavior in the process analysis section (Section 3.2). Although April 2019 daytime
288 ozone mixing ratios were higher than March 2019, we observed lower daytime ozone mixing ratios in
289 April 2020 compared with March 2020, both in the model and measured data. This may be seen in
290 contrast with what other studies that reported slightly higher ozone in Delhi during the lockdown
291 compared with pre-lockdown period (Jain & Sharma, 2020; Mahato et al., 2020). These differences are
292 primarily due to the methodology and the observed time period. For example, Jain and Sharma (2020)
293 reported an increase in daily ozone while we report the daytime ozone. On the other hand, Mahato et al.
294 (2020) looked at maximum daily 8-hour averaged (MDA8) ozone during two weeks in lockdown period

295 compared with two weeks in pre-lockdown period and reported less than 1% increase. Overall, the model
 296 was able to capture the major responses to the lockdown.



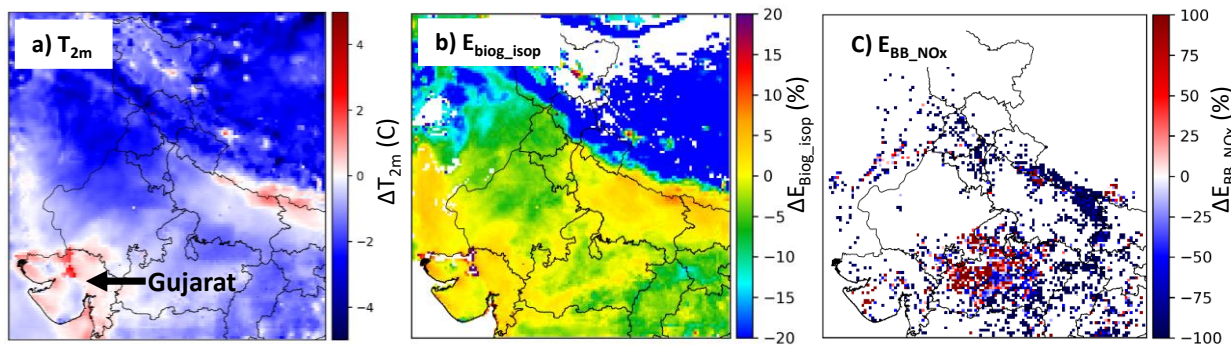
297
 298 Figure 4 Averaged daytime (1000-1700 LT) PM_{2.5} (top row), NO₂ (middle row), and ozone (bottom row) concentrations
 299 measured over CPCB stations in Delhi (left column) and modeled over Urban region (right column) between 10 March and 30
 300 April in 2019 (blue colors) and 2020 (red colors). The shaded regions show ± 1 STD. The observed data were extracted from the
 301 ground measurements data in Delhi, while the modeled data were averaged in the Urban subdomain.

302 3. Results

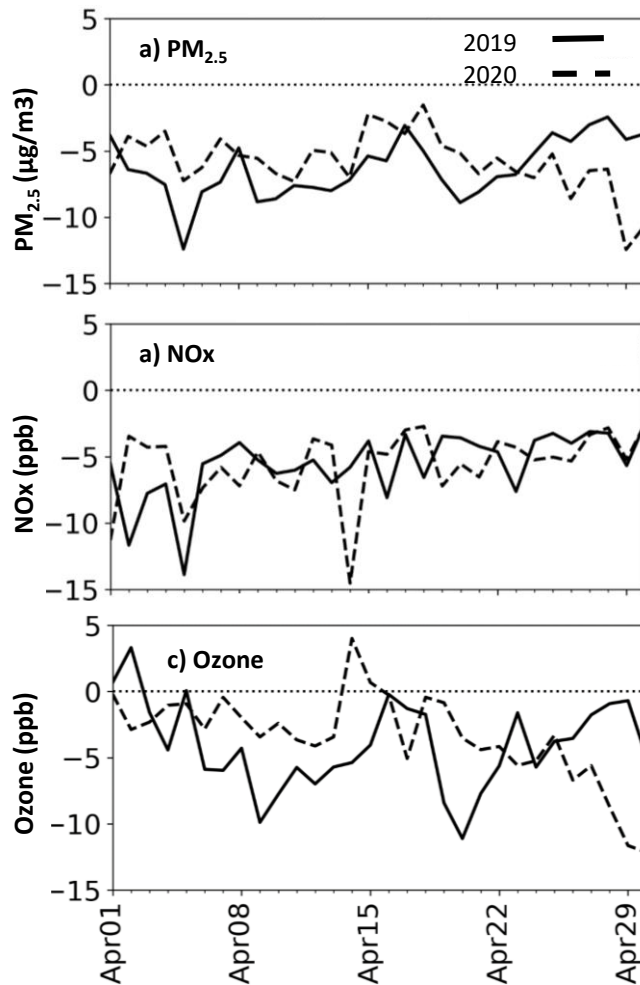
303 3.1. Model responses to Meteorology, Emission, and Combined 304 effects

305 To compare the air quality during the lockdown period (April 2020) with regards to the previous year, it
 306 is important to note that not only emissions but also the meteorology changed. Indeed, meteorology can
 307 affect both the transport of the pollution and natural sources emissions (i.e. biogenic and biomass burning
 308 emissions). Figure 5 shows the differences in 2-m temperature, biogenic isoprene emission, and biomass
 309 burning NO_x emission averaged during the daytime over the domain in April 2020 and April 2019. The
 310 western IGP had lower temperatures in April 2020 while eastern IGP and the state of Gujarat experienced
 311 warmer days. Because of higher temperatures, the online MEGAN module estimated by up to 10% more

312 biogenic isoprene emissions in eastern parts of the IGP in April 2020. On the other hand, it estimated by
 313 up to 10% lower isoprene emissions in western IGP in April 2020. Biomass burning emission in the IGP
 314 were lower in April 2020 with small fires in the eastern IGP. Overall, eastern IGP had higher biogenic
 315 emissions in April 2020, while biomass burning emissions were lower. In central India, biomass burning
 316 emissions were higher in April 2020 compared with April 2019. Due to such changes in meteorology and
 317 emissions, the effects of reducing anthropogenic emissions on regional air quality can be different
 318 depending on the applied year. Figure 6 shows the effects of emission reductions due to the lockdown in
 319 years 2019 (the difference between 2019COVID and 2019BAU scenarios) and 2020 (the difference
 320 between 2020COVID and 2020BAU scenarios) on averaged daytime $PM_{2.5}$, NO_x , and ozone in the Urban
 321 region. The averaged effect of emission perturbation on changes in daytime ozone concentration was -4.1
 322 ppb and -3.4 ppb in 2019 and 2020, respectively. Similarly, the effect of emission reductions on changes
 323 in daytime $PM_{2.5}$ concentration in 2019 was -6.3 $\mu g/m^3$ and was -5.8 $\mu g/m^3$ in 2020. For NO_x , the
 324 emission perturbation effect were similar in both 2019 and 2020. However, we found large differences in
 325 day-to-day comparison. For example, lockdown emissions in 2019 and 2020 decreased daytime $PM_{2.5}$
 326 concentrations in Urban by $\sim 12 \mu g/m^3$ and $\sim 7 \mu g/m^3$, respectively, on 5 April, which corresponds to
 327 $\sim 40\%$ difference due to the year applied. Moreover, the amount of reduction in NO_x mixing ratio on 14
 328 April was different by 46% (15 ppb and 7 ppb in 2019 and 2020, respectively). On the other hand, we
 329 also observed contradictory responses on some days. For example, ozone mixing ratios in Urban
 330 decreased on 14 April 2019 due to the lockdown emissions, while 2020 data showed an increase.



331
 332 Figure 5 Difference between April 2020 and 2019 in modeled daytime averaged a) 2-m temperature, b) biogenic isoprene, and c)
 333 biomass burning NO_x emissions over the domain



334

335

336

Figure 6 Effect of lockdown emissions on daytime a) PM_{2.5}, b) NO_x, and c) Ozone concentration in April 2019 (solid line; difference between 2019COVID and 2019BAU) and 2020 (dashed line; difference between 2020COVID and 2020BAU).

337

338

339

340

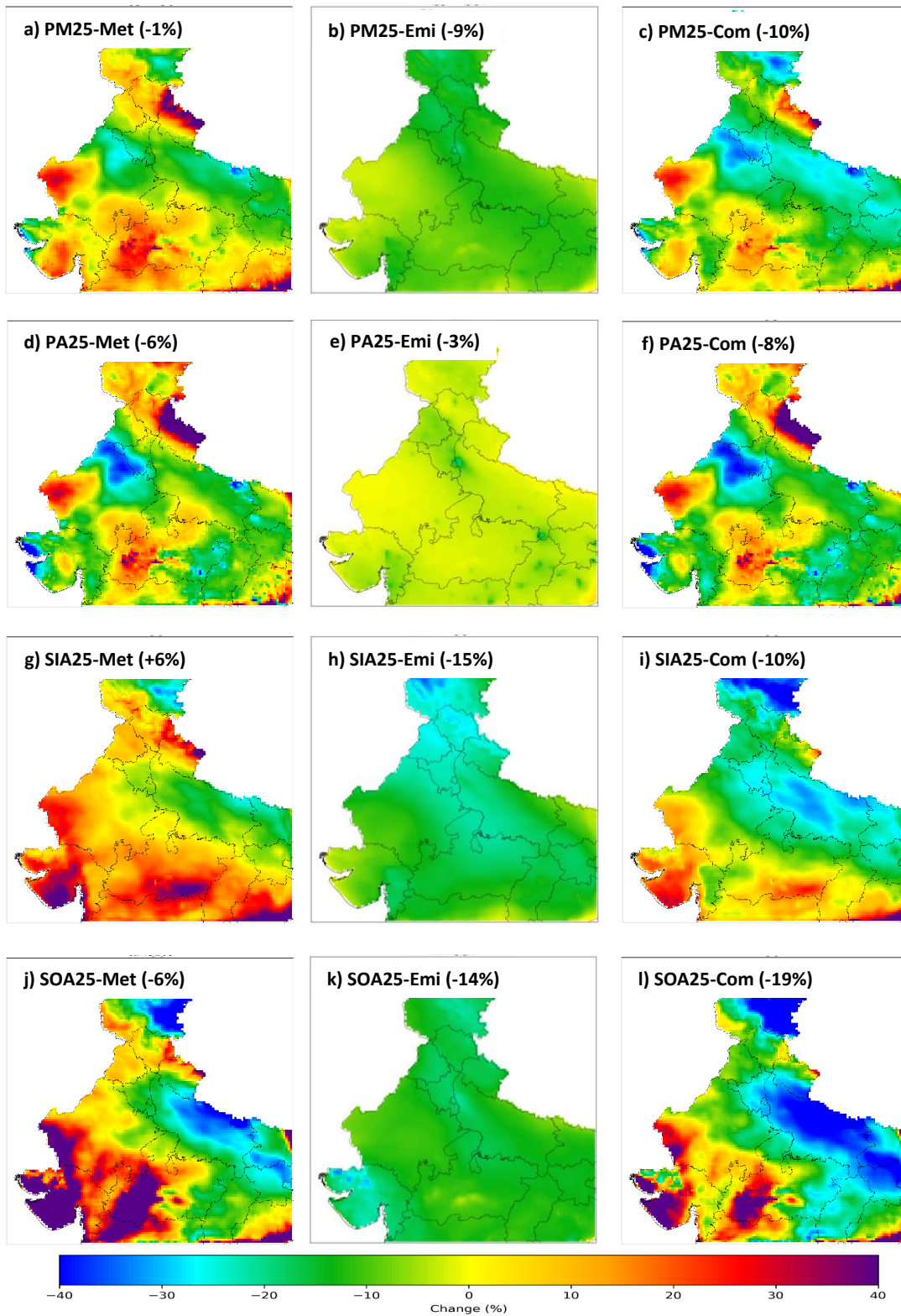
341

342

343

344

In order to attribute the changes between April 2019 and 2020, we looked at three scenarios. The difference between 2020BAU and 2019BAU indicates the effects of meteorology, while the difference between 2020COVID and 2020BAU presents the effects of lockdown emissions. Figure 7 and Figure 8 show the percentage of point-to-point changes due to meteorology, emissions, and their combined effects (the difference between 2020COVID and 2019BAU) on averaged daytime concentrations in April. In the following analysis, we focus only on India and disregard the changes over the boundaries (affected majorly by IC/BC) and over Himalayan region (very low concentrations). Similar plots for the IGP region is provided in the supporting information (Figure S6 and Figure S7).



345

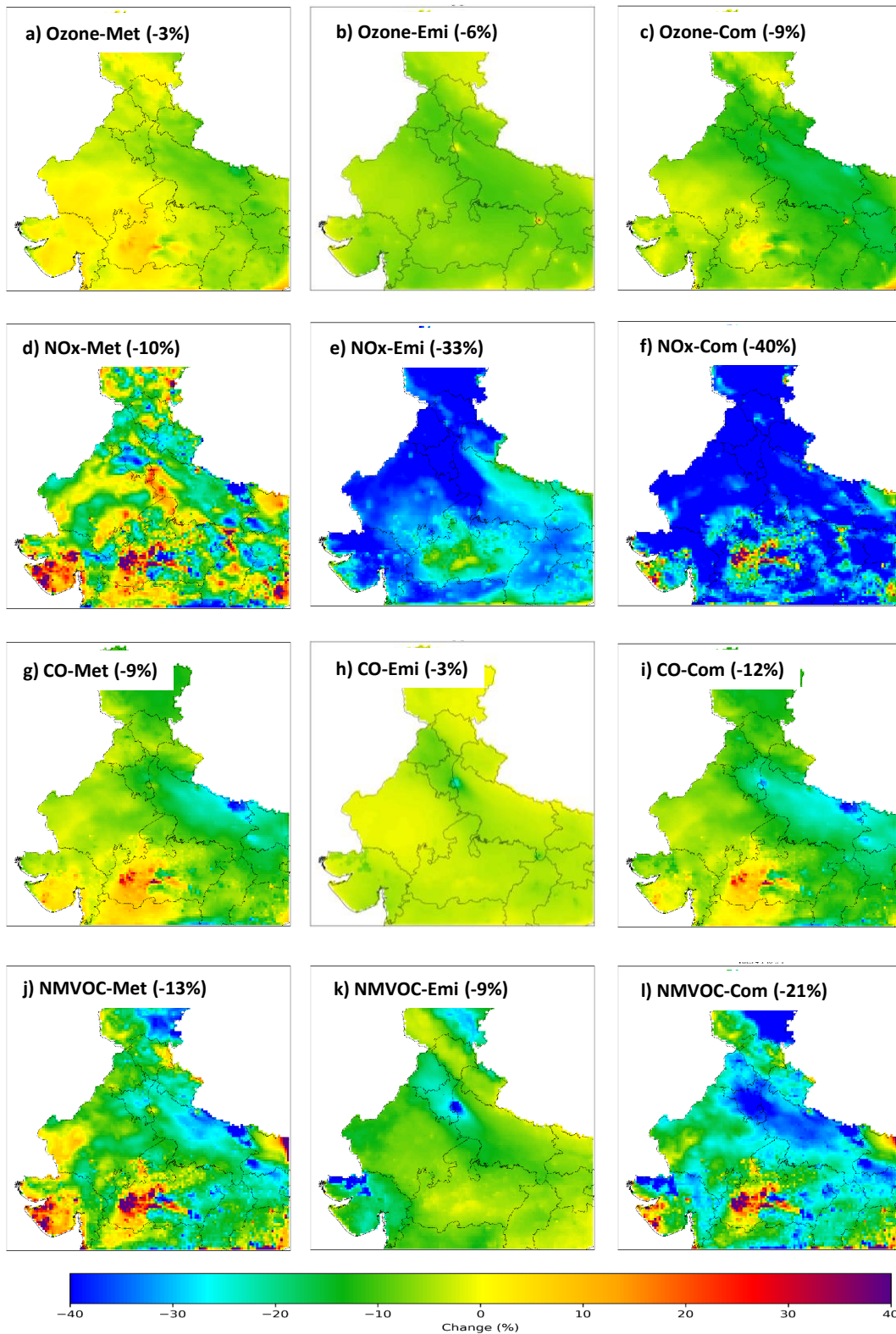
346

347

348

Figure 7 Responses of April averaged daytime PM_{2.5} (first row), PA_{2.5} (second row), SIA_{2.5} (third row), and SOA_{2.5} (fourth row) concentrations to meteorology (left column), emission (middle column), and combined (right column) effects. The numbers in the parenthesis show the averaged change over the colored region between April 2020 and 2019.

349 The averaged daytime PM_{2.5} concentrations in April in India decreased by only one percent due to the
350 meteorology effects. However, each region in the domain showed different changes. Figure 7 shows that
351 larger PM_{2.5} concentration reductions over the IGP due to the meteorology effects (Figure S6 shows 06%
352 for the IGP). The reduction was more intense in some parts of the IGP, e.g. west of Delhi (~25%). It also
353 shows PM_{2.5} concentrations increased over central India by more than 40% over the regions mostly
354 affected by biomass burning emissions. On the other hand, the lockdown emissions decreased PM_{2.5}
355 concentrations almost everywhere in India (i.e. the IGP and central India) with the average of 9% and the
356 maximum of ~20% in Delhi. The combined effects show a large reduction in PM_{2.5} concentrations over
357 the IGP (by up to 35%). However, the increase due to the meteorology over central India offset the
358 decrease due to the lockdown emissions. The changes in PM_{2.5} composition as primary aerosols (PA_{2.5};
359 sum of organic carbon, black carbon, and primary inorganics), secondary inorganic aerosols (SIA_{2.5}; sum
360 of nitrate, sulfate, and ammonium), and secondary organic aerosols (SOA_{2.5}) are also shown. All PM_{2.5}
361 constituents showed a reduction over eastern IGP and an increase over central India due to the
362 meteorology. The amount of changes were larger for SOA_{2.5} both in the eastern IGP and central India,
363 suggesting biomass burning emissions had larger impacts on SOAs. However PA_{2.5} decreased by up to
364 40% in the western IGP, while SOA_{2.5} and SIA_{2.5} changed by less than 10%. The large primary inorganics
365 component of PA_{2.5} and faster wind speeds on the border of India and Pakistan suggest that dust
366 emissions affected this region in April 2019 (Figure S8). Other studies have also reported pre-monsoon
367 windblown dusts over western India (R. Kumar et al., 2014; Sarkar et al., 2019). Lockdown emissions
368 decreased SIA_{2.5} and SOA_{2.5} between ~10-25% over the IGP with large changes over Delhi (~25%).
369 Similarly, PA_{2.5} decreased by ~10% over Delhi and surrounding areas. Similar reductions can be seen on
370 some other urban areas over the domain. However, lockdown emissions did not change PA_{2.5} very much
371 (<10%) in non-urban areas as AFs for BC in India (Figure 2) suggested. Furthermore, solid fuels are the
372 primary source of cooking and heating in non-urban regions in India and it did not change during the
373 lockdown period (Beig et al., 2021). The combined effects show larger impacts of meteorology on PA_{2.5}
374 and SOA_{2.5} in the IGP, while changes in emissions due to lockdown had larger impacts on SIA_{2.5} (Figure
375 S6).



376

377

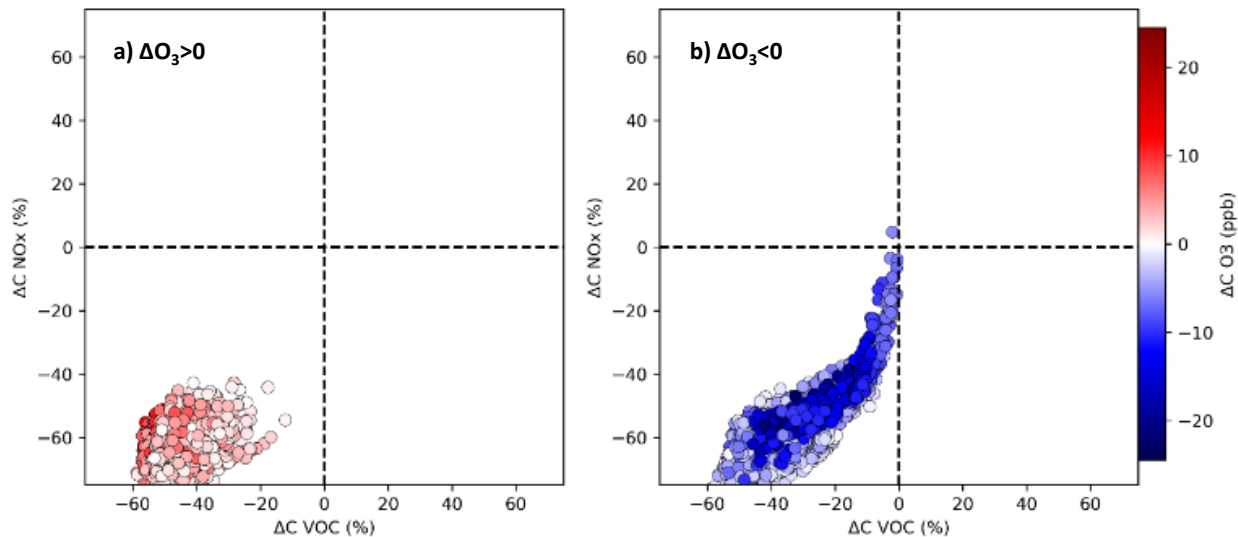
378

379

Figure 8 Responses of April averaged daytime ozone (first row), NOx (second row), CO (third row), and NMVOC (fourth row) concentrations to meteorology (left column), emission (middle column), and combined (right column) effects. The numbers in the parenthesis show the averaged change over the colored region between April 2020 and 2019.

380 In general, the effects of meteorology on ozone was similar to PM_{2.5}. Figure 8 shows that meteorology
381 effects led to lower (up to -20%) and higher (up to 20%) daytime ozone mixing ratios over the IGP and
382 central India, respectively. Regarding the ozone precursors, emission effects was significant for NO_x
383 concentration (-33%). Largely the changes in ozone can be explained by the changes in NO_x, as for most
384 parts of the domain ozone is NO_x-limited (as will be discussed in Section 3.2). For example, the changes
385 in NO_x emissions due to the lockdown are large and rather uniform over the domain. Throughout most of
386 the domain, NO_x concentrations due to emission perturbations decreased by over 30%. The ozone
387 decreases are strongly correlated with the regions with large NO_x decreases. We can see only the major
388 cities like Delhi and the regions with many power plants experienced increases in ozone mixing ratio with
389 decreases in NO_x emissions. On the other hand, ozone mixing ratio (combined effect) in the southern
390 parts of the domain increased although lockdown emissions reduced NO_x concentration. This is a region
391 where the NO_x concentrations increased due to meteorology (as shown in the change in NO_x-Met
392 subplot), which was due to the larger biomass burning emissions in April 2020 as shown in Figure 5. The
393 net effect is that NO_x concentrations increased in this region and this lead to higher ozone concentrations.
394 The meteorology effect on NMVOCs and CO concentrations shows lower concentrations over the IGP
395 and higher concentrations in central India in April 2020. While biogenic emissions were higher in the IGP
396 in April 2020, lower biomass burning emissions (as shown in Figure 5) explain the meteorology effects
397 on NMVOCs and CO concentrations in this region. Emission perturbations decreased NMVOCs
398 concentrations over India on average by 9%, while the reduction was ~40% in Delhi (similar to NO_x). The
399 effect of emissions on CO concentration was small over India (averaged reduction of 3%). This
400 magnitude was larger in Delhi (~25% reduction) and in lower magnitudes in other parts of the IGP. The
401 combined effects of meteorology and lockdown emissions on ozone and its precursors showed reduction
402 in daytime concentrations over all parts of India except central India. In central India, both biogenic
403 emissions and biomass burning emissions were higher in April 2020.

404 To better illustrate the response of ozone to changes in NO_x and NMVOC concentrations, we show the
405 response of the model in all the grid cells in Delhi (i.e. Urban) to the lockdown emission changes during
406 all daytime hours in April (Figure 9). In Delhi, daytime NMVOC concentrations decreased up to 60% and
407 NO_x concentrations decreased up to 70%. Ozone concentration showed both decreasing and increasing
408 response to the precursor reductions. Ozone increased in 20% of grid cells. In addition, most of these
409 increasing ozone data points belong to four (out of 20) grid cells located in the eastern part of the Urban
410 subdomain (not shown). It is important as local emission inventories also show Delhi (i.e. Urban) is most
411 densely populated in its eastern border. The largest increases were observed at NMVOC and NO_x
412 reductions of more than 40%. Power and Rural showed lower reductions in the precursor concentrations
413 and only a small number of grid cells showed an increased ozone response (Figure S9).



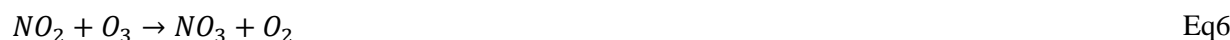
414
 415 Figure 9 Plot of changes in NO_x (Y-axis) and NMVOC (X-axis) concentrations due to the lockdown (2020COVID – 2020BAU)
 416 and ozone a) increasing and b) decreasing responses in all the grid cells within the Urban region (20 grid cells) during April (30
 417 days) daytime (1000-1700 LT) hours (total data points are 4800). X- and Y-axis are normalized values. 5th layer in the model was
 418 selected to minimize the impacts of direct emissions.

419 3.2. Process Analysis of ozone chemistry

420 As presented in the previous section, the changes in ozone concentrations did not exactly follow the
 421 changes in its precursors' emissions during the lockdown period. Specifically, NO_x and VOCs
 422 anthropogenic emissions were significantly decreased as a response to lockdown in India by up to 40%
 423 (Figure 2), whereas daytime ozone concentrations showed only a 6% reduction (Figure 8). More
 424 interestingly, 24-hour averaged ozone mixing ratios were higher on some days over Delhi during the
 425 lockdown period compared with the pre-lockdown period (Figure S5). In this section, we utilize the IRR
 426 capability of WRF-Chem to study the chemistry of ozone. We chose two sample days representing pre-
 427 lockdown and lockdown conditions to look at the ozone chemistry in previously-defined Urban, Power,
 428 and Rural regions. In order to choose these two days, we applied a meteorological filter in Urban to select
 429 the days with the most similar meteorology between years 2019 and 2020. We calculated the daytime
 430 averaged 10-meter wind speed and 2-meter temperature for each day in both years and found the day with
 431 lowest overall normalized biases (Figure S10). As a result, 13 March and 7 April were selected as the
 432 sample pre-lockdown and lockdown days, respectively. Nevertheless, it is important that these days were
 433 selected based on the filters in Urban and did not necessarily represented lowest-meteorological-
 434 variability days in Power and Rural (Figure S10). As an experiment, we applied the same methodology
 435 over India and found two other days with the least variability over the domain. However, it did not
 436 majorly affect the following analysis (not shown). We acknowledge that this technique of choosing the
 437 days does not consider the effects of previous days.

438 It is important to understand the general processes in the ozone chemistry; we provide a simplified
 439 overview of the complex chemistry of ozone in the troposphere. While NO_x and VOCs (including CO,
 440 and methane (CH₄)) are the main precursors of ozone, hydroxyl (OH) radical is also a key species in the
 441 ozone chemistry. The reason is that OH can oxidize VOCs and produce organic proxy radicals (RO₂) as
 442 shown in Eq1. Then, RO₂ can react with NO and produce NO₂ without involving ozone (Eq2: for
 443 simplicity, we do not show the pathway towards hydroperoxyl radical (HO₂) formation), which can

444 eventually lead to net ozone via Eq3 and Eq4. On the other hand, the ozone photolysis is the main source
 445 of tropospheric OH. Thus, this loop (Eq1 to Eq4) continues to form ozone during daytime ($h\nu$) as far as
 446 VOCs and OH are available in the atmosphere (NO_x acts more as a catalyst in this loop). Relative to
 447 VOCs, CO and CH₄ react very slowly with OH. Thus, short-lived VOCs become important as their
 448 availability primarily depend on their emissions. However, we should emphasize that it does not
 449 necessarily mean that large amounts of VOCs will increase ozone (i.e. radical loss via radicals (LRO_x)).
 450 In terms of OH, it can also react with NO₂ and form nitric acid (HNO₃), and remove both OH (and other
 451 radicals) and NO₂ (Eq5; this is the main reaction of radical loss via NO_x termination (LNO_x)). In other
 452 words, VOCs reactivity with OH (VOC+OH) shows a path to ozone formation (Eq1), and NO₂ reactivity
 453 with OH (NO₂+OH) presents an obstacle to ozone formation (Eq5). During nighttime, photolysis of NO₂
 454 (Eq3) does not occur, halting ozone formation cycle; rather, NO₂ reacts with ozone and form gas phase
 455 radical nitrate (NO₃) through Eq6. Moreover, available NO consumes ozone and produces NO₂ (Eq7),
 456 accelerating NO₃ chemistry, resulting in net ozone destruction. More detailed chemistry of ozone can be
 457 found elsewhere (e.g. Pusede and Cohen (2012); Seinfeld and Pandis (2016))



458

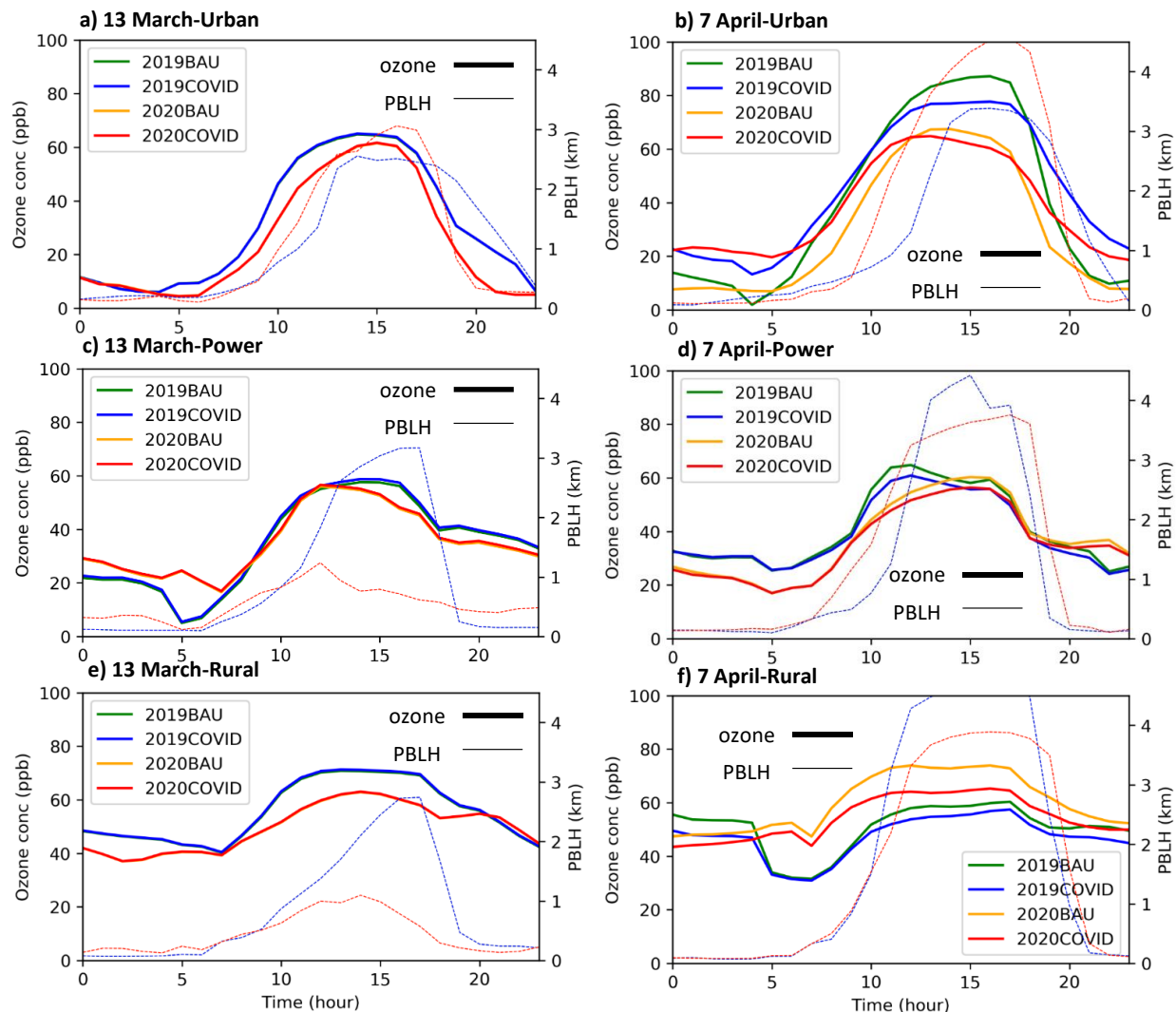
459 Figure 10 shows the surface ozone mixing ratio and planetary boundary layer height (PBLH) averaged
 460 within Urban, Power, and Rural regions for a pre-lockdown (13 March) and lockdown (7 April) days.
 461 First, we analyze the pre-lockdown day in Figure 10 (left column). It shows the differences within each
 462 region was only because of meteorology (2019 vs 2020). In Urban, the evolution of planetary boundary
 463 layer (PBL) was similar for both 2019 and 2020 scenarios and ozone followed similar trend as the PBL,
 464 with the peak at 1530 LT. In Power, the PBLH was lower in 2020 (1km) compared with 2019 (3km),
 465 which is consistent with this day's lower temperature and higher wind speed in 2020 (Figure S10).
 466 However, ozone mixing ratio were close to each other although peaked at different hours (1530 LT in
 467 2019 vs 1130 LT in 2020). Similarly in rural, models showed different PBL evolution, while ozone
 468 mixing ratio showed a smooth similar pattern between 2019 and 2020.

469 Second, we analyze the lockdown day (7 April) in Figure 10 (right column). In Delhi, the PBL grew
 470 faster and extended higher in 2020, while both years peaked during afternoon hours. The shallower PBLH
 471 in 2019 means more precursors are available in the shallower atmosphere (i.e. less dilution), leading to
 472 more ozone formation during the day. Moreover, the model simulated higher CO concentrations over the
 473 IGP in 2019 (not shown). Srinivas et al. (2016) found that transported pollution from the Bay of Bengal
 474 can potentially elevate the CO concentrations in Delhi. We are also interested in the impacts of lockdown
 475 emission. Comparing 2020BAU and 2020COVID, the lockdown resulted in lower peak value. It should
 476 be emphasized that this was not the case for the all days during the lockdown period as the impact of
 477 emissions on daytime ozone mixing ratio varied day by day in Urban (Figure 6). On the other hand, the

478 largest difference in ozone mixing ratio happens during 0030-0730 LT and 1830-2330 LT. While the
479 reaction between NO and ozone should deplete all the ozone in the atmosphere, the titration did not
480 deplete all the ozone in 2020COVID scenario due to lower amounts of NO available. As a result, some
481 residual ozone remained in the atmosphere.

482 In Power, the PBL grew faster in 2020 but its peak height was lower than 2019. However, the daytime
483 ozone mixing ratios did not change between both years (although the morning time (0830-1030 LT)
484 ozone was higher in 2019 due to lower PBLH). We also observed small changes between 2020BAU and
485 2020COVID scenarios. Although the percentage of emission changes were large for both VOCs and
486 NO_x, the amount of anthropogenic VOC emissions were low in this region and NO_x emissions in Power
487 were even more than Urban (Table S3). Furthermore, the eastern IGP was also significantly impacted by
488 biogenic emissions in 7 April 2020 (Figure S11). As a result, biogenic VOC emissions controlled the
489 ozone formation, which were similar in both 2020BAU and 2020COVID scenarios.

490 In Rural, the PBL growth in 2019 was faster and it extended higher than 2020. Figure S10 also shows that
491 wind speed in Rural was lower by ~75% on 7 April 2020 compared with the same day in 2019, leaning
492 towards a stagnant condition. As a result, the ozone mixing ratio is higher in 2020 scenarios. Comparing
493 2020BAU and 2020COVID shows a reduction during all hours due to the lockdown emissions.



494
 495 Figure 10 Surface ozone mixing ratio (primary Y-axis) and PBLH (secondary Y-axis) averaged over Urban (top row), Power
 496 (middle row), and Rural (bottom row) for a sampled pre-lockdown day (13 March: left column) and lockdown day (7 April: right
 497 column).

498 Figure 11 shows the OH reactivity with VOCs and NO₂ within Urban, Power, and Rural regions for a pre-
 499 lockdown (13 March) and lockdown (7 April) day. We followed Pfister et al. (2019) suggestion in
 500 averaging these values within the PBL to minimize the effects of mixing. It is important to note (1) these
 501 OH reactivity plots are averaged within the PBL, while ozone mixing ratios in Figure 10 were surface
 502 values and (2) these plots indicate the chemistry contribution to the ozone mixing ratio, while other
 503 contributing factors such as vertical mixing and advection are also important processes impacting the
 504 actual ozone mixing ratio (Pusede & Cohen, 2012).

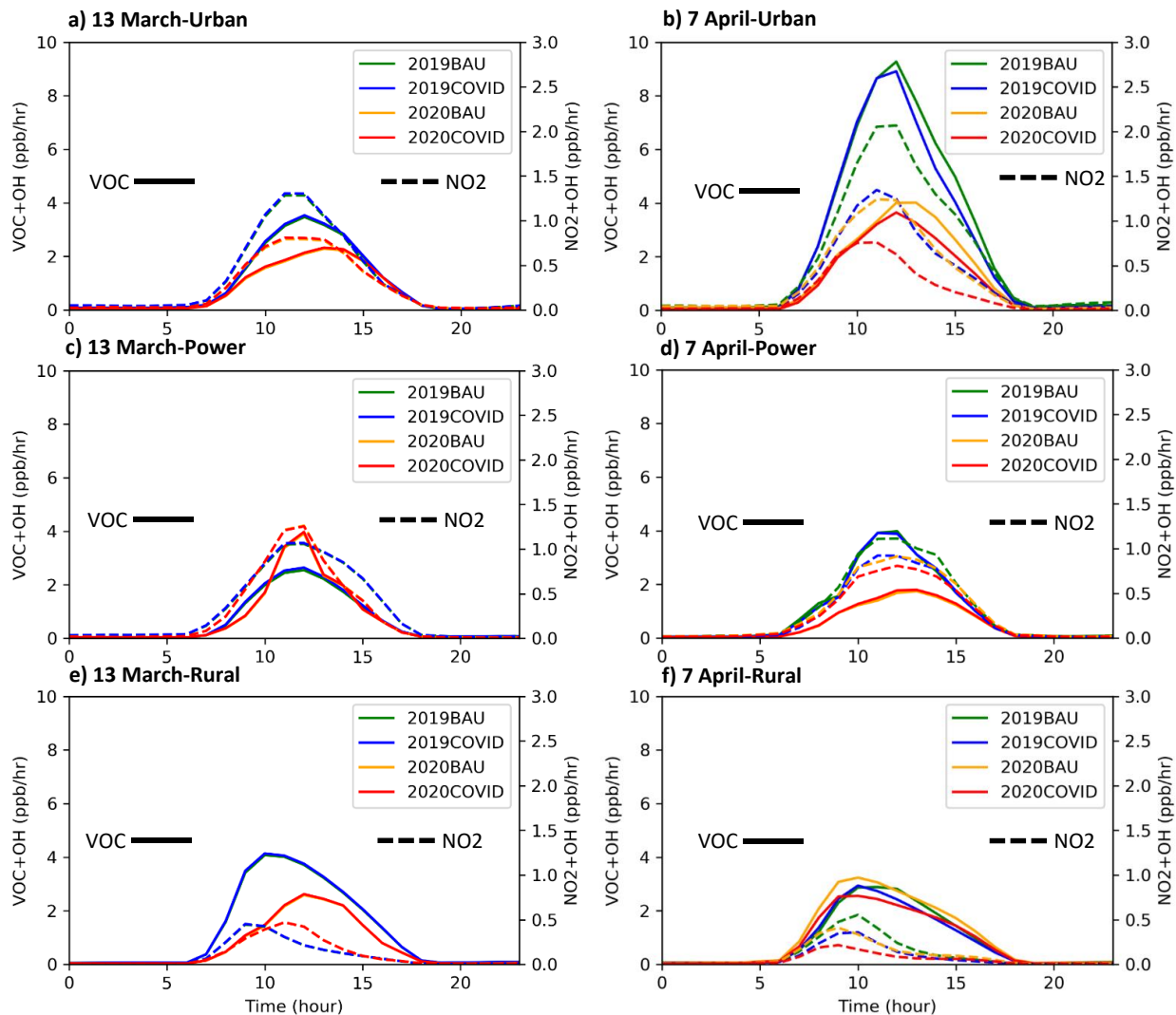
505 During the pre-lockdown day, VOC+OH and NO₂+OH were different for 2019 and 2020 in Urban.
 506 Although there were also some differences in the time of the peaks, the ratio of VOC+OH to NO₂+OH
 507 was similar, suggesting the ozone formation was not very much different. In Power, the VOC+OH
 508 increased in 2020, while the peak of NO₂+OH did not change. It shows that meteorology effects
 509 (including natural sources emissions) majorly affected OH reactivity with VOC in Power. In Rural, the

510 results showed smaller VOC+OH rates in 2020 with roughly similar NO₂+OH rates. However, both VOC
511 and NO_x anthropogenic emissions were low in this region and very similar between 2019 and 2020.
512 Similarly, it indicates the importance of meteorology effects and accompanied biogenic and biomass
513 burning emissions on the ozone formation in Rural.

514 During the lockdown day, OH reactivity (with both VOC and NO₂) was higher in 2019 scenarios than
515 2020 in Urban. This is consistent with shallower PBL in 2019, which led to higher ozone mixing ratios. In
516 2020 scenarios, the NO₂+OH rate dropped in 2020COVID compared with 2020BAU (0.5 ppb/hr), with
517 smaller reductions in VOC+OH rate (0.2 ppb/hr). Until 1230 LT, the model did not show any large
518 reductions in VOC+OH (i.e. ozone formation did not change), while NO₂+OH showed large drops (i.e.
519 ozone destruction decreased). Similarly, we saw larger surface ozone mixing ratios until noon in
520 2020COVID scenario. After 1230 LT, the VOC+OH showed larger reductions, leading to lower net
521 ozone formation in the 2020COVID scenario.

522 In Power, larger OH reactivity values were observed for both VOC and NO₂ in 2019 compared with
523 2020. This was unexpected as we observed larger biogenic isoprene emissions in 7 April 2020 (Figure
524 S11). However, it can be explained by higher CO contribution in 2019 results (Figure S12). On the other
525 hand, the biogenic soil NO emission was also larger in 2019; resulting in more ozone formation.
526 Considering the lockdown emissions, the model showed that adjusted emissions (i.e. COVID scenarios)
527 did not change VOC+OH values. This is due to low anthropogenic and equal biogenic VOC emissions in
528 this region. NO₂+OH values decreased as NO_x emissions reduced

529 In Rural, we observed similar behavior of OH reactivity for both 2019 and 2020. It is consistent with
530 similar ozone mixing ratio trend in Figure 10. As emissions are low in this region, ozone formation and
531 OH reactivity does not play an important role and ozone differences can be explained by dynamics and
532 atmospheric stability. As a result, adjusted emissions had similar effect on both VOC+OH and NO₂+OH
533 rates in 2020 scenarios.



534
 535 Figure 11 OH reactivity with VOCs (primary Y-axis) and NO₂ (secondary Y-axis) averaged within PBL over Urban (top row),
 536 Power (middle row), and Rural (bottom row) for a sampled pre-lockdown day (13 March: left column) and lockdown day (7
 537 April: right column).

538 Since there are many VOCs available in the atmosphere, IRR gives us the opportunity to find the species
 539 that have higher contributions to the OH reactivity. Figure S12 shows the OH reactivity for the top six
 540 VOC species for the lockdown day in each region and scenario. CO was the main component in all the
 541 regions and scenarios. Although CO reacts slowly in the atmosphere (i.e. long lifetime), its abundant
 542 availability moves it to the top of the list. The other species were short-lived species. Formaldehyde
 543 (CH₂O) was the second-ranked species in almost all the subfigures except the ones that isoprene (ISOP)
 544 had more reactivity rate. Specifically, ISOP was the second-ranked species in Power region in all the
 545 scenarios. This is because VOCs in Power region were dominated with biogenic sources and changing the
 546 anthropogenic emissions did not change their rankings. Regardless, the meteorology affected the
 547 magnitude of the contribution between the two years. ISOP was also the second-ranked species in Urban
 548 in 2020COVID scenario. High contributions by CO and CH₂O to OH reactivity is also reported in the
 549 United States (Pfister et al., 2019). They found that high contribution of CH₂O to OH reactivity was due

550 to both local emissions and chemical production, while ISOP was mostly due to biogenic emissions.
551 While CH₂O had larger contribution in the Urban, ISOP had larger contributions in the Power, which is
552 consistent with Pfister et al. (2019). In Urban, the transportation sector had the largest contribution in
553 anthropogenic emissions of CH₂O (~90%) and residential sector had about 10% of its emission. We also
554 found contributions from the large alkenes (BIGENE), which is a tracer of anthropogenic VOCs, in BAU
555 scenarios in Power. Comparing the ranking of ISOP in 2020BAU and 2020COVID for Urban shows
556 biogenic emissions had a larger contribution during the lockdown. It points to the need to consider the
557 background biogenic emissions when evaluating expected changes in ozone due to anthropogenic
558 emissions reductions. Large alkanes (BIGALK) contributed to the OH reactivity over Urban in 2019BAU
559 and 2020BAU and over Rural in 2020BAU. BIGALK is another tracer of anthropogenic VOCs, and its
560 contribution in Rural indicates the impact of transport on ozone mixing ratio in this region. Analysis of
561 the HTAP emission inventory revealed that the transportation sector has the largest BIGALK and
562 BIGENE emissions in Urban (~90%). The second-ranked anthropogenic sector in Urban was the
563 industrial sector for BIGALK emission and residential sector for BIGENE emission. When looking at the
564 entire domain (i.e. India region), transportation sector had the largest BIGALK emission, while the
565 residential sector had the largest contribution for BIGENE and CH₂O emission.

566 As discussed earlier, LRO_x and LNO_x are the reactions that determine the radical terminations by
567 radicals and NO_x, respectively, during the daytime (Table S6 and Table S7). More information on IRR
568 analysis methodology is provided in the supporting information. The LRO_x/LNO_x ratio is very important
569 from policy's perspective as it indicates whether reduction in NO_x (large ratio values; i.e. NO_x-limited)
570 or VOCs (small ratio values; i.e. VOC-limited) emission is the efficient strategy for ozone reduction.
571 Duncan et al. (2010) assumed the transition between NO_x-limited and VOC-limited regions happens at a
572 LRO_x/LNO_x ratio of one. Schroeder et al. (2017) found the transition of ozone production occurs at a
573 ratio of 0.35 using 0-D photochemical box modeling. However, evaluating the LRO_x and LNO_x values is
574 not usually possible based on observations. As a result Sillman (1995) proposed using the ratio of
575 measured tracers in the atmosphere as an alternative. The formaldehyde to NO₂ ratio (FNR) is one of the
576 most frequently used ratio as its species can be measured from both ground measurements and space
577 borne instruments (Jin & Holloway, 2015; V. Kumar et al., 2020; Martin et al., 2004). Mahajan et al.
578 (2015) used the FNR transition range between one and two to study the inter-annual variations of ozone
579 formation in India using satellite observations, whereas Schroeder et al. (2017) showed this transition
580 range is not constant in all regions. For example, they found in their box modeling study in the US that
581 the transition range was 0.9-1.80 in Colorado, while the range of 0.7-2.0 was found for Houston, Texas.
582 In other words, the FNR transition range for each region should be exclusively specified for each region.

583 Figure 12 shows the plots of FNR ratio within the PBL as a function of LRO_x/LNO_x in Urban, Power,
584 and Rural for the 2019BAU and 2020BAU scenarios during the afternoon hours (1230-1430 LT). The
585 results for 2019BAU (2020BAU) show that 65% (67%) of points were in the VOC-limited region (i.e.
586 LRO_x/LNO_x<0.35) in Delhi, whereas only 1% (2%) of the points were in the VOC-limited region in
587 Rural. These results show that ozone formation regime differs for each region and indicate that we cannot
588 employ one uniform emission control strategy everywhere in the IGP (and India). The results for Delhi
589 support the idea that the emission control strategies that target the transportation sector, with the primary
590 goal of PM reduction, can increase ozone (Chen et al., 2020). In Power, 64% (65% for 2020BAU) of the
591 data-points were in the VOC-limited region, which is expected as this domain had low amounts of
592 anthropogenic VOCs emissions (Table S3) and biogenic emissions were the primary source VOCs
593 (Figure S12), suggesting extreme NO_x emission reduction may be the only solution in this region. While
594 the effect of different meteorology (2019BAU vs 2020BAU) on chemical regimes were negligible,
595 dramatic changes in emissions can lead to large changes. For example, only 34% of points were in the

596 VOC-limited regime in Urban for 2020COVID scenario, in which both NMVOC and NO_x emissions had
597 large reductions (Figure S13).

598 Calculating binned averages and corresponding standard deviations for the FNR data can provide some
599 insights about the transition range (Schroeder et al., 2017). We also took the union of the transition range
600 of 2019BAU and 2020BAU scenarios to minimize the effect of meteorology. In Urban, our results
601 suggest that the FNR transition range is 0.4-1.1. However, it is clear that this range covers a large amount
602 of data points in other bins as well. In Power, the lower range of the transition range goes to zero due to
603 the large amounts of NO_x emissions in this region. However, the upper range (1.2) can be used as a cut-
604 off between VOC- and NO_x-limited regimes in Power. In Rural, the transition range is 0.7-1.3, which was
605 derived based on less than 5% of the data. We also observed larger LRO_x/LNO_x ratios in Rural compared
606 with other regions, indicating the role of biogenic emissions in non-urban regions. Schroeder et al. (2017)
607 emphasized that other parameters (e.g. different radicals with different lifetimes than formaldehyde) can
608 affect the FNR ratio and it may not be a solid indicator of ozone formation sensitivity in some regions.
609 Furthermore, Souri et al. (2020) studied the functionality of FNR ratio and found situations where
610 LRO_x/LNO_x and FNR lead to contradicting conclusions regarding the chemical regime in a region,
611 primarily because of impacts of NO₂ on formaldehyde.

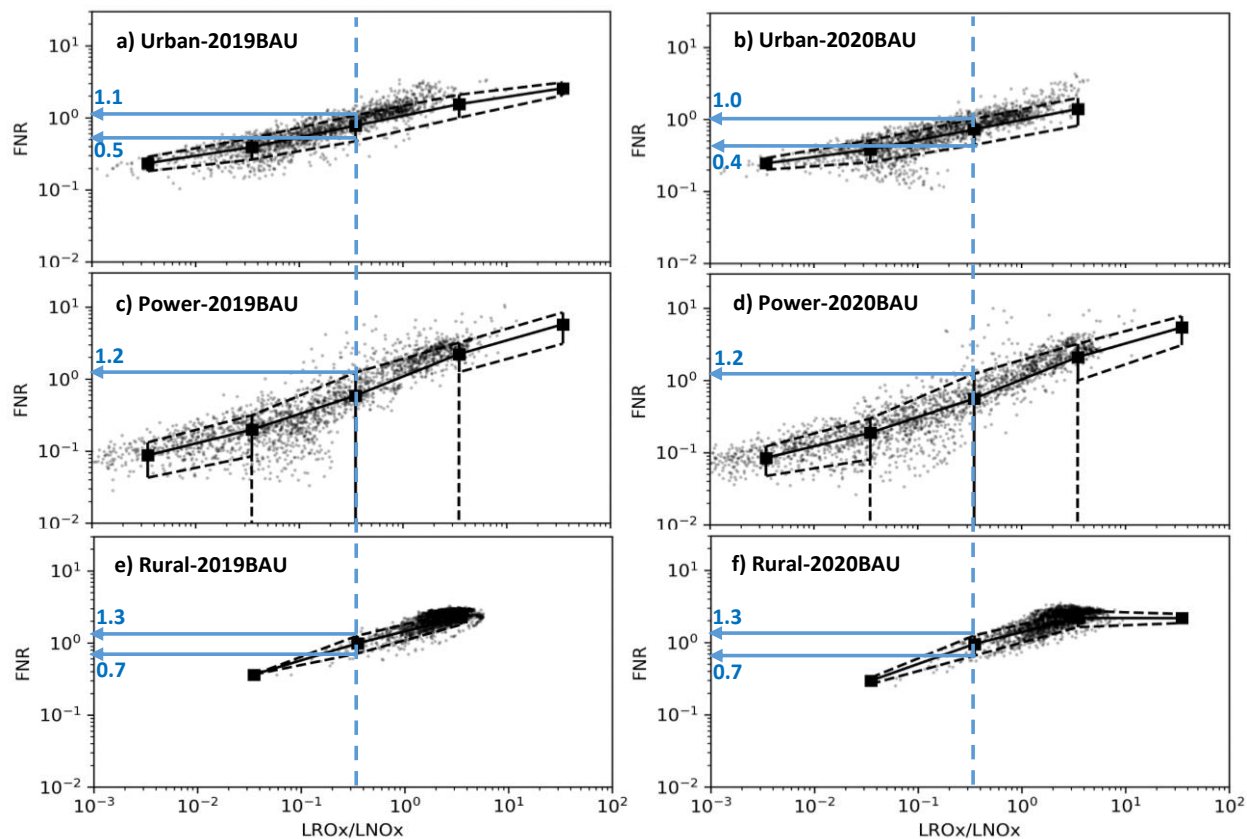
612 Figure 13 shows the FNR ratio using 2020BAU and 2020COVID scenarios averaged in Urban, Power,
613 and Rural during afternoon hours (1230-1430 LT) in April 2020. In Urban, 29 days were estimated to be
614 in the transition range in 2020BAU scenario, while they were mostly close to the lower limit of the
615 transition range (i.e. toward VOC-limited). Applying the lockdown emissions increased the FNR ratio by
616 an average value of 0.48 and shifted almost all the days into either a NO_x-limited or an upper limit of the
617 transition range. Although it slightly changed the ozone formation regime, we did not see any major
618 change in daytime ozone concentration in Urban (Figure S14). In Power using 2020BAU scenario, we
619 observed that only four days in April were completely in a NO_x-limited regime while the FNR in rest of
620 the days were lower than the upper-limit of the transition region. The FNR ratio increased by an average
621 value of 0.21 because of lockdown emissions reductions (i.e. 2020COVID). However, about half of the
622 days remained below the upper-limit of the transition and did not moved to NO_x-limited region, showing
623 the lockdown emissions did not majorly change the ozone formation chemistry in Power. In Rural, almost
624 all the days (28 days) were already in the NO_x-limited regime in 2020BAU scenario. As a result,
625 increasing the FNR ratio by an average value of 0.49 due to the lockdown emissions (i.e. 2020COVID)
626 did not change the ozone formation chemistry in Rural.

627 Using the upper-limit of the calculated transition regime (1.3) in the three mentioned regions, we looked
628 at the ozone production regimes for the entire study domain (Figure 14). We found that most parts of
629 India are in the NO_x-limited regime. Indeed, all the regions except the urban areas, power plant region,
630 and western IGP fall in the NO_x-limited regime. The FNR in Haryana state was lower than 1.3, showing
631 the state is in the VOC-limited regime. There are some locations in Punjab state with VOC-limited regime
632 (FNR<1.3), while other locations are slightly in NO_x-limited regime. Likewise, there are some locations
633 (cities) in Uttar Pradesh with FNR close to 1.3 (i.e. close to VOC-limited regime). Using the lockdown
634 emissions (2020COVID), the FNR increased over the domain, moving most parts of the Punjab and
635 Haryana states into NO_x-limited regime. On the other hand, the FNR in some urban locations (e.g. Delhi)
636 and the Power region remained below 1.3; the ozone production regime did not change. Overall, our
637 analysis indicate that the FNR can determine a region that is strictly NO_x- or VOC-limited (e.g. Power
638 and Rural) but caution should be exercised for regions close to the defined transition regions (e.g. Urban).

639 Comparing the total OH consumed by each pathway (i.e. integrating the 24-hr values in Figure 11 for 7
640 April as the lockdown day) and their ratio in 2020BAU and 2020COVID scenarios can also provide some

641 information on whether ozone chemistry regime changed because of the lockdown. Table S8 shows
 642 integrated values in total OH consumption by VOCs was higher in Urban and Rural compared with
 643 Power, confirming low VOCs in Power region. Moreover, the ratio of total OH consumption by VOC to
 644 NO_2 had smallest values in Power, showing the preference of $\text{NO}_2 + \text{OH}$ pathway in this region.
 645 Evaluating the change of the ratio because of lockdown emissions indicates that Urban and Rural shifted
 646 toward NO_x limited regime, while the ozone chemistry regime did not change in Power.

647



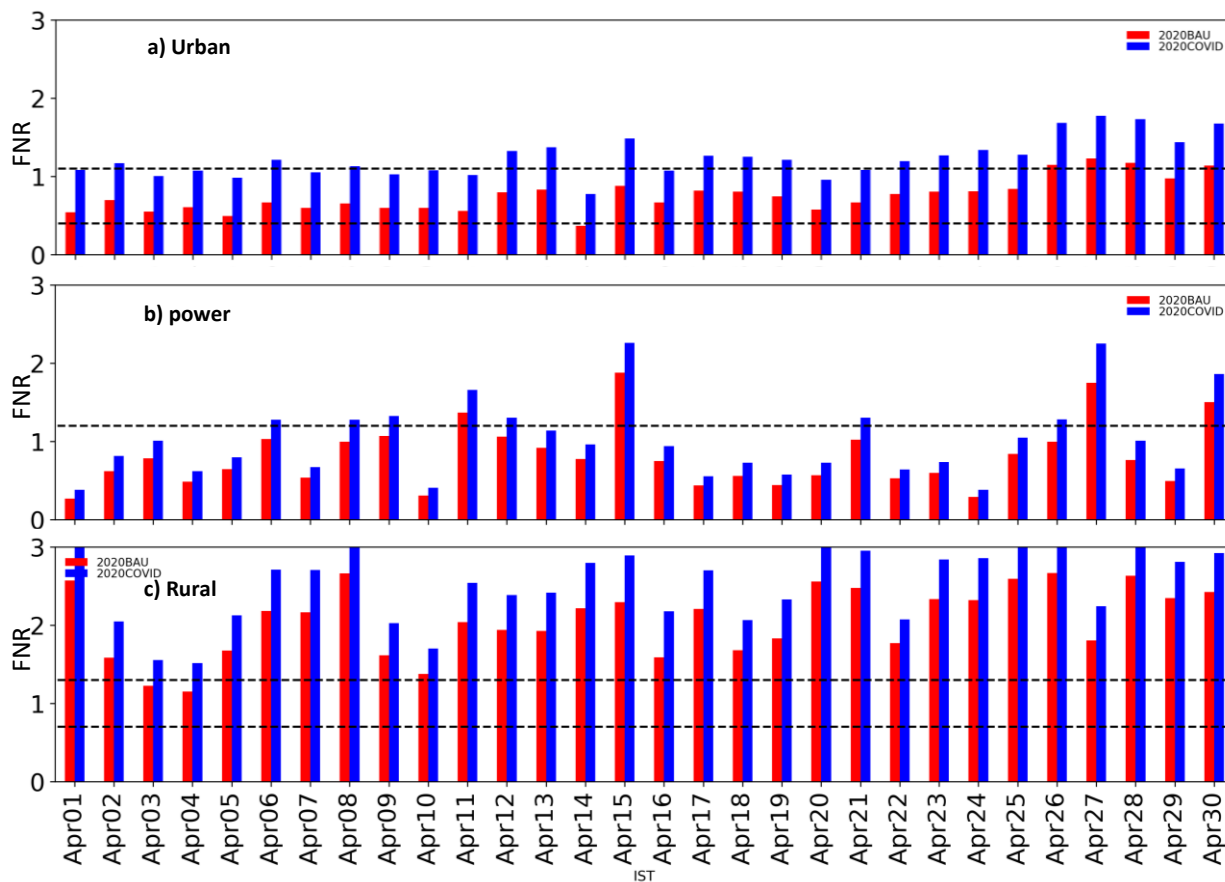
648

649

650 Figure 12 Plots of point-to-point FNR ratio (within the PBL) as a function of LROx/LNO_x ratio during afternoon hours (1230-
 651 1430 LT) for 2019BAU (left column) and 2020BAU (right column) scenarios in a, b) Urban, c, d) Power, and e, f) Rural regions.

652 Binned averages (black squares) and standard deviations (vertical black bars) were calculated. The vertical dashed blue line
 653 represents LROx/LNO_x ratio of 0.35. The horizontal blue vectors show the FNR transition range in each region (numbers in blue
 654 show the values).

655

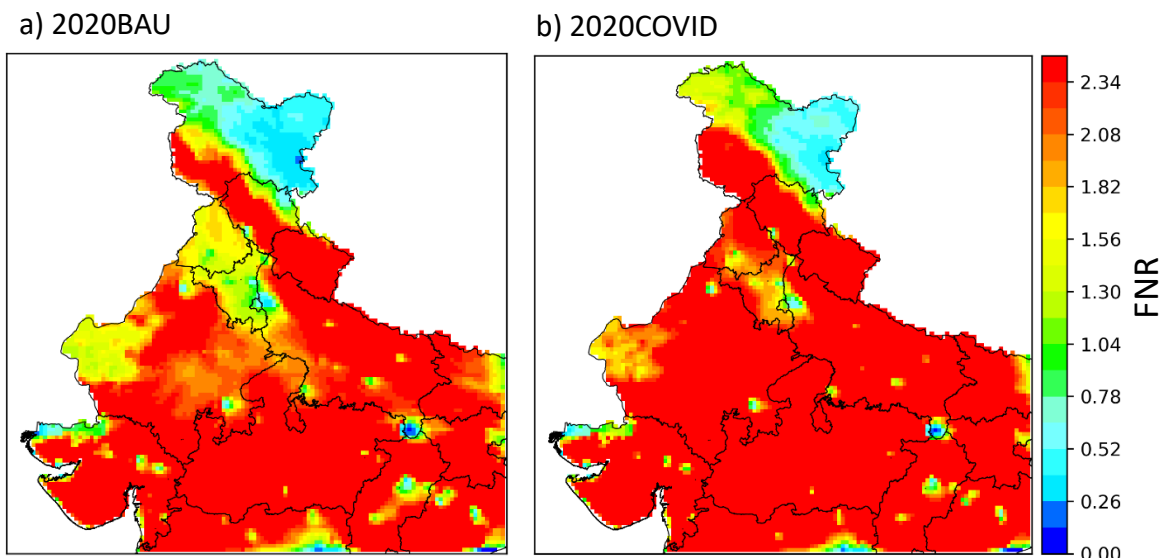


656

657 Figure 13 FNR ratio within the PBL averaged during afternoon (1230-1430 LT) in a) Urban, b) Power, and c) Rural regions.

658 Dashed horizontal line in each panel represents the transition range calculated based on LROx/LNOx ratio analysis.

659



660

661

Figure 14 FNR ratio (within the PBL) averaged over April using a) 2020BAU and b) 2020COVID scenarios.

662 4. Summary and Conclusion

663 We studied the effects of COVID-19 stay-at-home orders (i.e. lockdown) on northern India's air quality
 664 and explored the chemistry behind the changes in ozone concentrations. For this purpose, we used the
 665 WRF-Chem version 4.0 model to utilize its integrated reaction rate (IRR) capability. The adjustment
 666 factors proposed by Doumbia et al. (2021) were used to account for the anthropogenic emission changes
 667 during the lockdown period in India. While the model satisfied the benchmark criteria proposed by Emery
 668 et al. (2017) for daily $PM_{2.5}$ concentration in Delhi, it overestimated (underestimated) the daytime ozone
 669 (NO_2 and CO) concentrations against the CPCB ground measurements data. However, the model was able
 670 to capture the overall observed trend in air pollutant concentrations in 2019 and 2020.

671 Four scenarios were designed to study the effect of the meteorology and lockdown anthropogenic
 672 emission perturbations in April 2019 and 2020. We found that the effects of perturbing the anthropogenic
 673 emissions could be different depending on the applied year. The reason is that not only the anthropogenic
 674 emissions but also the meteorological dependent emissions (e.g. biogenic emissions) and the atmospheric
 675 dynamics affect the air quality in a region. We also estimated the changes in air pollutant concentrations
 676 between April 2019 and 2020 and the contribution of meteorology and lockdown emissions. While the
 677 $PM_{2.5}$ concentration averaged over the IGP decreased by 6% in April 2020 due to the meteorology, it
 678 increased in the central India due to more biomass burning emissions. However, the lockdown emissions
 679 decreased the $PM_{2.5}$ concentration over Indian parts of the domain by 9%. For ozone, we found the
 680 meteorology decreased the concentrations over the IGP and increased it over the central India, similar to
 681 $PM_{2.5}$. However, the ozone concentration response to its precursors (i.e. NO_2 and VOCs) significant
 682 reductions due to the lockdown emissions was not constant over the domain. While ozone decreased in
 683 most parts of the domain, we saw that major cities like Delhi and the regions with many power plants
 684 showed increases in ozone with decreases in NO_x emissions.

685 We also analyzed the ozone chemistry in an urban, a rural, and a densely populated power plants region
 686 during a sampled pre-lockdown and lockdown day. Using OH reactivity with VOCs (NO_2) as the pathway
 687 to ozone formation (destruction), we found that the lockdown emissions decreased both pathways in the

688 urban and rural region. However, it only decreased the ozone destruction in the power plant region
689 (NO_2+OH) and did not affect the ozone formation path ($\text{VOC}+\text{OH}$), as natural emission sources
690 dominated the VOC emissions in this region. Our analysis showed that CO had the highest contribution in
691 the net ozone production in all the regions and all the scenarios. We also found formaldehyde, isoprene,
692 acetaldehyde, and ethylene contributed to the ozone formation in all the regions. However, the magnitude
693 of contribution depended on the region and scenario. While formaldehyde was the second ranked VOC in
694 the urban region in a business as usual scenario in 2020, isoprene had larger contribution in the lockdown
695 scenario, indicating the impact of biogenic emissions in that region. We also found higher alkanes and
696 higher alkenes, as tracers of anthropogenic emissions, contributed to the ozone formation in the rural
697 region, indicating the effect of the transport in ozone formation.

698 Furthermore, we calculated the rates that radicals (i.e. HO_2 and RO_2) react with radicals (i.e. LRO_x) or
699 NO_2 (i.e. LNO_x) and used their ratio ($\text{LRO}_x/\text{LNO}_x$) to find the ozone chemistry regime in different
700 regions. Our analysis showed that the urban and power plant regions were primarily VOC-limited
701 ($\text{LRO}_x/\text{LNO}_x < 0.35$), while the rural region was in NO_x -limited region. Following Schroeder et al.
702 (2017), we also calculated this ratio's corresponding formaldehyde to NO_2 concentration ratio (FNR) in
703 each region. This is preferred as it can be calculated using ground measurements and satellite observation
704 data. Our analysis suggested the FNR ratio of 1.3 as the upper-limit of the transition regime from VOC-
705 limited to NO_x -limited over India. Using that threshold, we classified most parts of India in the NO_x -
706 limited regime while most of the cities like Delhi and power plant region are in the VOC-limited regime.
707 Some regions like the western IGP were towards the VOC-limited regime but shifted to NO_x -limited
708 regime after applying the lockdown emissions.

709 Understanding the ozone formation chemistry and the role of emission sources and different species can
710 help the policy makers to implement efficient emission control scenarios. Our results showed that the
711 ozone formation process can be different in each region depending on its local anthropogenic and natural
712 emission sources and the meteorology. We acknowledge that our study was limited to only three arbitrary
713 chosen regions. While our results can provide information on overall response of the air quality to
714 emission reductions, they do not necessarily represent the general ozone chemistry in India. However, it
715 provides a framework that can be used to study the efficacy of local emission control scenarios on ozone
716 formation in India.

717 **Data Availability** The WRF-Chem and IRR hourly output results for all four scenarios are
718 available from Iowa Research Online at <https://doi.org/10.25820/data.006144>. TROPOMI data can be
719 freely downloaded from the European Space Agency Copernicus Open Access Hub
720 (<https://doi.org/10.5270/S5P-s4ljg54>). MERRA-2 data can be freely downloaded from NASA EarthData
721 Portal (<https://earthdata.nasa.gov/>).

722 **Acknowledgements** This work was funded in part by NASA HAQAST and ACPMAP projects
723 under awards NNX16AQ19G and 80NSSC19K094, respectively. BR also acknowledges supports from
724 the university of Iowa graduate college summer fellowship. All the calculations and simulations are done
725 using the University of Iowa Argon high-performance computing cluster. BR and GRC designed the
726 research; BR performed all the model simulations; SKG provided measurements data; BR and MAO
727 analyzed the IRR outputs. BR and GRC wrote the paper. All authors contributed to discussion and edited
728 the paper. The authors declare that they have no conflict of interest.

729

730 References

- 731 Abdi-Oskouei, M., Pfister, G., Flocke, F., Sobhani, N., Saide, P., Fried, A., Richter, D., Weibring, P.,
732 Walega, J., & Carmichael, G. (2018). Impacts of physical parameterization on prediction of
733 ethane concentrations for oil and gas emissions in WRF-Chem. *Atmospheric Chemistry and*
734 *Physics*, 18(23), 16863-16883.
- 735 Amann, M., Kiesewetter, G., Schöpp, W., Klimont, Z., Winiwarter, W., Cofala, J., Rafaj, P., Höglund-
736 Isaksson, L., Gomez-Sabriana, A., & Heyes, C. (2020). Reducing global air pollution: the scope
737 for further policy interventions. *Philosophical Transactions of the Royal Society A*, 378(2183),
738 20190331.
- 739 Beig, G., Korhale, N., Rathod, A., Maji, S., Sahu, S. K., Dole, S., Latha, R., & Murthy, B. (2021). On
740 modelling growing menace of household emissions under COVID-19 in Indian metros.
741 *Environmental pollution*, 272, 115993.
- 742 Biswal, A., Singh, V., Singh, S., Kesarkar, A. P., Ravindra, K., Sokhi, R. S., Chipperfield, M. P.,
743 Dhomse, S. S., Pope, R. J., & Singh, T. (2020). COVID-19 lockdown induced changes in NO₂
744 levels across India observed by multi-satellite and surface observations. *Atmospheric Chemistry*
745 *and Physics Discussions*, 1-28.
- 746 Bosilovich, M., Lucchesi, R., & Suarez, M. (2015). MERRA-2: File specification.
- 747 Chen, Y., Beig, G., Archer-Nicholls, S., Drysdale, W., Acton, W. J. F., Lowe, D., Nelson, B., Lee, J.,
748 Ran, L., & Wang, Y. (2020). Avoiding high ozone pollution in Delhi, India. *Faraday*
749 *Discussions*.
- 750 Conibear, L. (2018). *Ambient air quality and human health in India*. (Doctor of Philosophy), University
751 of Leeds, University of Leeds.
- 752 Conibear, L., Butt, E. W., Knotte, C., Spracklen, D. V., & Arnold, S. R. (2018). Current and Future
753 Disease Burden From Ambient Ozone Exposure in India. *GeoHealth*, 2(11), 334-355.
- 754 Doumbia, T., Granier, C., Elguindi, N., Bouarar, I., Darras, S., Brasseur, G., Gaubert, B., Liu, Y., Shi, X.,
755 & Stavrou, T. (2021). Changes in global air pollutant emissions during the COVID-19
756 pandemic: a dataset for atmospheric chemistry modeling. *Earth System Science Data*
757 *Discussions*, 1-26.
- 758 Dumka, U., Kaskaoutis, D., Verma, S., Ningombam, S. S., Kumar, S., & Ghosh, S. (2021). Silver linings
759 in the dark clouds of COVID-19: Improvement of air quality over India and Delhi metropolitan
760 area from measurements and WRF-CHIMERE model simulations. *Atmospheric Pollution*
761 *Research*, 12(2), 225-242.
- 762 Duncan, B. N., Yoshida, Y., Olson, J. R., Sillman, S., Martin, R. V., Lamsal, L., Hu, Y., Pickering, K. E.,
763 Retscher, C., & Allen, D. J. (2010). Application of OMI observations to a space-based indicator
764 of NO_x and VOC controls on surface ozone formation. *Atmospheric Environment*, 44(18), 2213-
765 2223.
- 766 Emery, C., Liu, Z., Russell, A. G., Odman, M. T., Yarwood, G., & Kumar, N. (2017). Recommendations
767 on statistics and benchmarks to assess photochemical model performance. *Journal of the Air &*
768 *Waste Management Association*, 67(5), 582-598.
- 769 Emery, C., Tai, E., & Yarwood, G. (2001). Enhanced meteorological modeling and performance
770 evaluation for two Texas ozone episodes. *Prepared for the Texas natural resource conservation*
771 *commission, by ENVIRON International Corporation*.
- 772 Emmons, L. K., Schwantes, R. H., Orlando, J. J., Tyndall, G., Kinnison, D., Lamarque, J. F., Marsh, D.,
773 Mills, M. J., Tilmes, S., & Bardeen, C. (2020). The chemistry mechanism in the Community
774 Earth System Model version 2 (CESM2). *Journal of Advances in Modeling Earth Systems*, 12(4).
- 775 Emmons, L. K., Walters, S., Hess, P. G., Lamarque, J.-F., Pfister, G. G., Fillmore, D., Granier, C.,
776 Guenther, A., Kinnison, D., & Laepple, T. (2010). Description and evaluation of the Model for
777 Ozone and Related chemical Tracers, version 4 (MOZART-4).

778 ESA. (2020). Air pollution drops in India following lockdown. Retrieved from
779 [https://www.esa.int/Applications/Observing_the_Earth/Copernicus/Sentinel-](https://www.esa.int/Applications/Observing_the_Earth/Copernicus/Sentinel-5P/Air_pollution_drops_in_India_following_lockdown#.YFzj-71W1ss.link)
780 [5P/Air_pollution_drops_in_India_following_lockdown#.YFzj-71W1ss.link](https://www.esa.int/Applications/Observing_the_Earth/Copernicus/Sentinel-5P/Air_pollution_drops_in_India_following_lockdown#.YFzj-71W1ss.link)

781 Garaga, R., Sahu, S. K., & Kota, S. H. (2018). A review of air quality modeling studies in India: local and
782 regional scale. *Current Pollution Reports*, 4(2), 59-73.

783 Gaubert, B., Bouarar, I., Doumbia, T., Liu, Y., Stavrakou, T., Deroubaix, A. M., Darras, S., Elguindi, N.,
784 Granier, C., & Lacey, F. G. (2020). Global Changes in Secondary Atmospheric Pollutants during
785 the 2020 COVID-19 Pandemic. *Earth and Space Science Open Archive ESSOAr*.

786 Ghude, S. D., Chate, D., Jena, C., Beig, G., Kumar, R., Barth, M., Pfister, G., Fadnavis, S., & Pithani, P.
787 (2016). Premature mortality in India due to PM_{2.5} and ozone exposure. *Geophysical Research*
788 *Letters*, 43(9), 4650-4658.

789 Ghude, S. D., Jena, C., Chate, D., Beig, G., Pfister, G., Kumar, R., & Ramanathan, V. (2014). Reductions
790 in India's crop yield due to ozone. *Geophysical Research Letters*, 41(15), 5685-5691.

791 Gkatzelis, G. I., Gilman, J. B., Brown, S. S., Eskes, H., Gomes, A. R., Lange, A. C., McDonald, B. C.,
792 Peischl, J., Petzold, A., Thompson, C. R., & Kiendler-Scharr, A. (2021). The global impacts of
793 COVID-19 lockdowns on urban air pollution: A critical review and recommendations. *Elementa:*
794 *Science of the Anthropocene*, 9(1). doi:10.1525/elementa.2021.00176

795 Goldberg, D. L., Anenberg, S. C., Griffin, D., McLinden, C. A., Lu, Z., & Streets, D. G. (2020).
796 Disentangling the impact of the COVID-19 lockdowns on urban NO₂ from natural variability.
797 *Geophysical Research Letters*, 47(17), e2020GL089269.

798 Goldberg, D. L., Saide, P. E., Lamsal, L. N., Foy, B. d., Lu, Z., Woo, J.-H., Kim, Y., Kim, J., Gao, M., &
799 Carmichael, G. (2019). A top-down assessment using OMI NO₂ suggests an underestimate in the
800 NO_x emissions inventory in Seoul, South Korea, during KORUS-AQ. *Atmospheric Chemistry*
801 *and Physics*, 19(3), 1801-1818.

802 Gorris, M. E., Anenberg, S. C., Goldberg, D. L., Kerr, G. H., Stowell, J. D., Tong, D., & Zaitchik, B. F.
803 (2021). Shaping the future of science: COVID-19 highlighting the importance of GeoHealth.
804 *Earth and Space Science Open Archive ESSOAr*.

805 Granier, C., Darras, S., van der Gon, H. D., Jana, D., Elguindi, N., Bo, G., Michael, G., Marc, G.,
806 Jalkanen, J.-P., & Kuenen, J. (2019). *The Copernicus atmosphere monitoring service global and*
807 *regional emissions (April 2019 version)*. Copernicus Atmosphere Monitoring Service,

808 Grell, G. A., Peckham, S. E., Schmitz, R., McKeen, S. A., Frost, G., Skamarock, W. C., & Eder, B.
809 (2005). Fully coupled “online” chemistry within the WRF model. *Atmospheric Environment*,
810 39(37), 6957-6975.

811 Guenther, A., Karl, T., Harley, P., Wiedinmyer, C., Palmer, P., & Geron, C. (2006). Estimates of global
812 terrestrial isoprene emissions using MEGAN (Model of Emissions of Gases and Aerosols from
813 Nature). *Atmospheric Chemistry and Physics*, 6(11), 3181-3210.

814 Gupta, S. (2020). Air pollution in northern India has hit a 20-year low, NASA report says. *CNN*.

815 HEI. (2018). *Burden of Disease Attributable to Major Air Pollution Sources in India*. Retrieved from

816 Hodzic, A., & Jimenez, J. (2011). Modeling anthropogenically controlled secondary organic aerosols in a
817 megacity: A simplified framework for global and climate models. *Geoscientific Model*
818 *Development*, 4(4), 901-917.

819 Hodzic, A., Madronich, S., Kasibhatla, P., Tyndall, G., Aumont, B., Jimenez, J., Lee-Taylor, J., &
820 Orlando, J. (2015). Organic photolysis reactions in tropospheric aerosols: effect on secondary
821 organic aerosol formation and lifetime. *Atmospheric Chemistry and Physics*, 15(16), 9253-9269.

822 Jain, S., & Sharma, T. (2020). Social and travel lockdown impact considering coronavirus disease
823 (COVID-19) on air quality in megacities of India: Present benefits, future challenges and way
824 forward. *Aerosol and air quality research*, 20(6), 1222-1236.

825 Janssens-Maenhout, G., Crippa, M., Guizzardi, D., Dentener, F., Muntean, M., Pouliot, G., Keating, T.,
826 Zhang, Q., Kurokawa, J., & Wankmüller, R. (2015). HTAP_v2. 2: a mosaic of regional and
827 global emission grid maps for 2008 and 2010 to study hemispheric transport of air pollution.
828 *Atmospheric Chemistry and Physics*, 15(19), 11411-11432.

829 Jena, C., Ghude, S. D., Kulkarni, R., Debnath, S., Kumar, R., Soni, V. K., Acharja, P., Kulkarni, S. H.,
830 Khare, M., & Kaginalkar, A. J. (2020). Evaluating the sensitivity of fine particulate matter (PM
831 2.5) simulations to chemical mechanism in Delhi. *Atmospheric Chemistry and Physics*
832 *Discussions*, 1-28.

833 Jin, X., & Holloway, T. (2015). Spatial and temporal variability of ozone sensitivity over China observed
834 from the Ozone Monitoring Instrument. *Journal of Geophysical Research: Atmospheres*, 120(14),
835 7229-7246.

836 Knote, C., Hodzic, A., Jimenez, J., Volkamer, R., Orlando, J., Baidar, S., Brioude, J., Fast, J., Gentner,
837 D., & Goldstein, A. (2014). Simulation of semi-explicit mechanisms of SOA formation from
838 glyoxal in aerosol in a 3-D model. *Atmospheric Chemistry and Physics*, 14(12), 6213-6239.

839 Kota, S. H., Guo, H., Myllyvirta, L., Hu, J., Sahu, S. K., Garaga, R., Ying, Q., Gao, A., Dahiya, S., &
840 Wang, Y. (2018). Year-long simulation of gaseous and particulate air pollutants in India.
841 *Atmospheric Environment*, 180, 244-255.

842 Kumar, R., Barth, M., Pfister, G., Naja, M., & Brasseur, G. (2014). WRF-Chem simulations of a typical
843 pre-monsoon dust storm in northern India: influences on aerosol optical properties and radiation
844 budget. *Atmos. Chem. Phys*, 14(5), 2431-2446.

845 Kumar, R., Naja, M., Pfister, G., Barth, M., Wiedinmyer, C., & Brasseur, G. (2012). Simulations over
846 South Asia using the Weather Research and Forecasting model with Chemistry (WRF-Chem):
847 chemistry evaluation and initial results. *Geoscientific Model Development*, 5(3), 619-648.

848 Kumar, V., Beirle, S., Dörner, S., Mishra, A. K., Donner, S., Wang, Y., Sinha, V., & Wagner, T. (2020).
849 Long-term MAX-DOAS measurements of NO₂, HCHO, and aerosols and evaluation of
850 corresponding satellite data products over Mohali in the Indo-Gangetic Plain. *Atmospheric*
851 *Chemistry and Physics*, 20(22), 14183-14235.

852 Kumari, P., & Toshniwal, D. (2020). Impact of lockdown measures during COVID-19 on air quality—A
853 case study of India. *International journal of environmental health research*, 1-8.

854 Mahajan, A. S., De Smedt, I., Biswas, M. S., Ghude, S., Fadnavis, S., Roy, C., & van Roozendael, M.
855 (2015). Inter-annual variations in satellite observations of nitrogen dioxide and formaldehyde
856 over India. *Atmospheric Environment*, 116, 194-201.

857 Mahato, S., Pal, S., & Ghosh, K. G. (2020). Effect of lockdown amid COVID-19 pandemic on air quality
858 of the megacity Delhi, India. *Science of the total environment*, 730, 139086.

859 Martin, R. V., Fiore, A. M., & Van Donkelaar, A. (2004). Space-based diagnosis of surface ozone
860 sensitivity to anthropogenic emissions. *Geophysical Research Letters*, 31(6).

861 Miyazaki, K., Bowman, K., Sekiya, T., Takigawa, M., Neu, J. L., Sudo, K., Osterman, G., & Eskes, H.
862 (2020). Global tropospheric ozone responses to reduced NO_x emissions linked to the COVID-19
863 world-wide lockdowns. *Earth and Space Science Open Archive ESSOAr*.

864 Mor, S., Kumar, S., Singh, T., Dogra, S., Pandey, V., & Ravindra, K. (2021). Impact of COVID-19
865 lockdown on air quality in Chandigarh, India: understanding the emission sources during
866 controlled anthropogenic activities. *Chemosphere*, 263, 127978.

867 Pfister, G., Wang, C. T., Barth, M., Flocke, F., Vizuete, W., & Walters, S. (2019). Chemical
868 Characteristics and Ozone Production in the Northern Colorado Front Range. *Journal of*
869 *Geophysical Research: Atmospheres*, 124(23), 13397-13419.

870 Pommier, M., Fagerli, H., Gauss, M., Simpson, D., Sharma, S., Sinha, V., Ghude, S. D., Landgren, O.,
871 Nyiri, A., & Wind, P. (2018). Impact of regional climate change and future emission scenarios on
872 surface O₃ and PM 2.5 over India. *Atmospheric Chemistry and Physics*, 18(1), 103-127.

873 Pusede, S., & Cohen, R. (2012). On the observed response of ozone to NO_x and VOC reactivity
874 reductions in San Joaquin Valley California 1995–present. *Atmospheric Chemistry and Physics*,
875 12(18), 8323-8339.

876 Roozitalab, B., Carmichael, G. R., & Guttikunda, S. K. (2021). Improving regional air quality predictions
877 in the Indo-Gangetic Plain—case study of an intensive pollution episode in November 2017.
878 *Atmospheric Chemistry and Physics*, 21(4), 2837-2860.

879 Sarkar, S., Chauhan, A., Kumar, R., & Singh, R. P. (2019). Impact of deadly dust storms (May 2018) on
880 air quality, meteorological, and atmospheric parameters over the northern parts of India.
881 *GeoHealth*, 3(3), 67-80.

882 Schroeder, J. R., Crawford, J. H., Fried, A., Walega, J., Weinheimer, A., Wisthaler, A., Müller, M.,
883 Mikoviny, T., Chen, G., & Shook, M. (2017). New insights into the column CH₂O/NO₂ ratio as
884 an indicator of near-surface ozone sensitivity. *Journal of Geophysical Research: Atmospheres*,
885 122(16), 8885-8907.

886 Seinfeld, J. H., & Pandis, S. N. (2016). *Atmospheric chemistry and physics: from air pollution to climate*
887 *change*: John Wiley & Sons.

888 Selvam, S., Muthukumar, P., Venkatramanan, S., Roy, P., Bharath, K. M., & Jesuraja, K. (2020). SARS-
889 CoV-2 pandemic lockdown: effects on air quality in the industrialized Gujarat state of India.
890 *Science of the total environment*, 737, 140391.

891 Sharma, A., Ojha, N., Pozzer, A., Mar, K. A., Beig, G., Lelieveld, J., & Gunthe, S. S. (2017). WRF-Chem
892 simulated surface ozone over south Asia during the pre-monsoon: effects of emission inventories
893 and chemical mechanisms. *Atmospheric Chemistry and Physics*, 17(23), 14393-14413.

894 Shi, X., & Brasseur, G. P. (2020). The response in air quality to the reduction of Chinese economic
895 activities during the COVID-19 outbreak. *Geophysical Research Letters*, 47(11),
896 e2020GL088070.

897 Sicard, P., De Marco, A., Agathokleous, E., Feng, Z., Xu, X., Paoletti, E., Rodriguez, J. J. D., &
898 Calatayud, V. (2020). Amplified ozone pollution in cities during the COVID-19 lockdown.
899 *Science of the total environment*, 735, 139542.

900 Sillman, S. (1995). The use of NO_y, H₂O₂, and HNO₃ as indicators for ozone-NO_x-hydrocarbon
901 sensitivity in urban locations. *Journal of Geophysical Research: Atmospheres*, 100(D7), 14175-
902 14188.

903 Singh, V., Singh, S., Biswal, A., Kesarkar, A. P., Mor, S., & Ravindra, K. (2020). Diurnal and temporal
904 changes in air pollution during COVID-19 strict lockdown over different regions of India.
905 *Environmental pollution*, 266, 115368.

906 Souri, A. H., Chance, K., Bak, J., Nowlan, C. R., González Abad, G., Jung, Y., Wong, D. C., Mao, J., &
907 Liu, X. (2021). Unraveling Pathways of Elevated Ozone Induced by the 2020 Lockdown in
908 Europe by an Observationally Constrained Regional Model: Non-Linear Joint Inversion of NO_x
909 and VOC Emissions using TROPOMI. *Atmospheric Chemistry and Physics Discussions*, 1-45.

910 Souri, A. H., Nowlan, C. R., Wolfe, G. M., Lamsal, L. N., Miller, C. E. C., Abad, G. G., Janz, S. J., Fried,
911 A., Blake, D. R., & Weinheimer, A. J. (2020). Revisiting the effectiveness of HCHO/NO₂ ratios
912 for inferring ozone sensitivity to its precursors using high resolution airborne remote sensing
913 observations in a high ozone episode during the KORUS-AQ campaign. *Atmospheric*
914 *Environment*, 224, 117341.

915 Srinivas, R., Beig, G., & Peshin, S. K. (2016). Role of transport in elevated CO levels over Delhi during
916 onset phase of monsoon. *Atmospheric Environment*, 140, 234-241.

917 Vadrevu, K. P., Eaturu, A., Biswas, S., Lasko, K., Sahu, S., Garg, J., & Justice, C. (2020). Spatial and
918 temporal variations of air pollution over 41 cities of India during the COVID-19 lockdown
919 period. *Scientific reports*, 10(1), 1-15.

920 *Whole Atmosphere Community Climate Model (WACCM) Model Output*. (2020). Retrieved from:
921 <https://rda.ucar.edu/datasets/ds313.6/>

922 Wiedinmyer, C., Akagi, S., Yokelson, R. J., Emmons, L., Al-Saadi, J., Orlando, J., & Soja, A. (2011).
923 The Fire INventory from NCAR (FINN): A high resolution global model to estimate the
924 emissions from open burning. *Geoscientific Model Development*, 4(3), 625.

925 Yadav, R., Korhale, N., Anand, V., Rathod, A., Bano, S., Shinde, R., Latha, R., Sahu, S., Murthy, B., &
926 Beig, G. (2020). COVID-19 lockdown and air quality of SAFAR-India metro cities. *Urban*
927 *Climate*, 34, 100729.

928 Zaveri, R. A., Easter, R. C., Fast, J. D., & Peters, L. K. (2008). Model for simulating aerosol interactions
929 and chemistry (MOSAIC). *Journal of Geophysical Research: Atmospheres*, 113(D13).

930 Zhang, M., Katiyar, A., Zhu, S., Shen, J., Xia, M., Ma, J., Kota, S. H., Wang, P., & Zhang, H. (2021).
931 Impact of reduced anthropogenic emissions during COVID-19 on air quality in India.
932 *Atmospheric Chemistry and Physics*, 21(5), 4025-4037.

933 **References from the Supporting Information**

934 Guttikunda, S. K., Nishadh, K., and Jawahar, P.: Air pollution knowledge assessments (APnA) for 20
935 Indian cities, *Urban Climate*, 27, 124-141, 2019.
936 Jena, C., Ghude, S. D., Kumar, R., Debnath, S., Govardhan, G., Soni, V. K., Kulkarni, S. H., Beig, G.,
937 Nanjundiah, R. S., and Rajeevan, M.: Performance of high resolution (400 m) PM 2.5 forecast over Delhi,
938 *Scientific reports*, 11, 1-9, 2021.
939
940

Elucidating the Impacts of COVID-19 Lockdown on Air Quality and Ozone Chemical Characteristics in IndiaBehrooz Roozitalab^{1,2}, Gregory R. Carmichael^{1,2}, Sarath K. Guttikunda³, Maryam Abdi-Oskouei⁴¹Center for Global and Regional Environmental Research, University of Iowa, Iowa City, IA, USA²Chemical and Biochemical Engineering, University of Iowa, Iowa City, IA, USA³Urban Emissions, New Delhi, India⁴University Corporation for Atmospheric Research (UCAR), Boulder, CO, USA**Contents of this file**

Text S1 to S2

Figures S1 to S15

Tables S1 to S8

Introduction

The supporting information includes an overview of comparison between the results using HTAP v2.2 and CAMS v4.2 emission inventories (Text S1), a guideline how to use the IRR outputs of WRF-Chem model (Text S2), and figures and tables supporting the results in the main manuscript.

Text S1- Comparing results using HTAP v2.2 and CAMS v4.2 anthropogenic emission inventories

To evaluate how changing anthropogenic emission inventories affect simulation results, we performed a set of experiments using HTAP v2.2 and the Copernicus Atmosphere Monitoring Service global emission inventory version 4.2 (CAMS v4.2) available from ECCAD database (<https://permalink.aeris-data.fr/CAMS-GLOB-ANT>, last access: 02/23/2021). CAMS v4.2 provides 0.1x0.1 degree gridded monthly-averaged emissions for the years between 2000 and 2020. It uses Emissions Database for Global Atmospheric Research version 4.3.2 (EDGARv4.3.2) for the years before 2012 and projects emissions between 2012 and 2020 using the Community Emissions Data System (CEDS) emission trends (Granier et al., 2019). Comparing CAMS v4.2 and HTAP v2.2 emissions for Delhi (i.e. Urban) indicated about 100% and 200% higher BC and OC emissions, respectively, in CAMS v4.2 inventory. CAMS v4.2 also showed higher CO (32%) emission, while lower NO_x (23%) and SO₂ (12%) emissions. NMVOC emissions was roughly similar in both inventories.

Statistics using CAMS v4.2 emission inventory were improved (Table S4-S5). In April 2019, the NMB for daily PM_{2.5} and daytime ozone decreased by 10% and 12%, respectively. In April 2020, the NMB for daily PM_{2.5} decreased by 47% and decreased by 10% for daytime ozone. Overall, the model performance using both emission inventories were within the benchmark criteria for daily PM_{2.5} concentrations. Moreover, the performance for daytime ozone concentration was similar using both inventories. Although there are some local emission inventories available throughout the country (Guttikunda et al., 2019; Jena et al., 2021), this experiment showed the necessity of an updated gridded national emission inventory for India. Regardless, our primary goal in this study was to investigate how the emission changes affected concentrations changes rather than capturing the actual concentrations. Results using CAMS emissions are very similar to those using HTAP as Figure S15 shows.

Text S2. Using IRR data in WRF-Chem model

IRR provides the gas-phase reaction rate for the species involved in each reaction. As a simple unit for these outputs, IRR within the WRF-Chem model, are in ppb and are cumulative. As a result, the hourly reaction rates (ppb/hr) can be calculated by subtracting the values in two consecutive hours. We use the difference between hours “i” and “i+1” as the reaction rate in hour “i”. Reporting this information in ‘ppb/hr’ makes the data easy-to-report and useful for all the species within the reaction. For example, in the reaction $A+B \rightarrow C+D$, a single reaction rate of RR in ppb/hr shows that RR ppb of A and B was consumed and RR ppb of C and D was produced in a specific hour. In our analysis, we used the IRR information averaged within the boundary layer following Pfister et al. (2019).

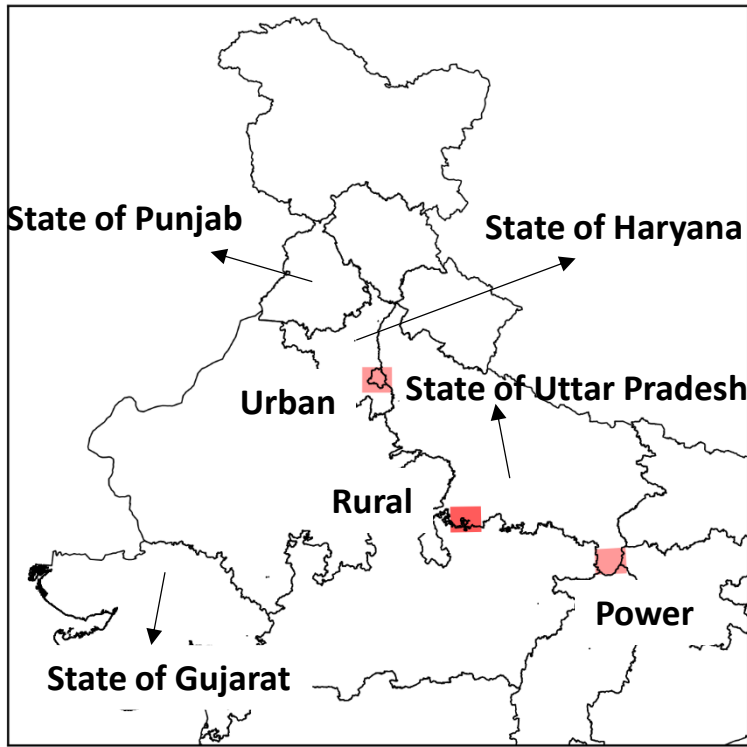


Figure S1 Location of the selected regions of Urban (Lower Left (LL): 28.3N, 76.7E, Upper Right (UR): 28.9N, 77.5E), Rural (LL: 25N, 79E, UR: 25.6N, 79.8E), and Power (LL: 23.9N, 82.7E, UR: 24.5N, 83.5E). States of Punjab, Haryana, Uttar Pradesh, and Gujarat are also shown.

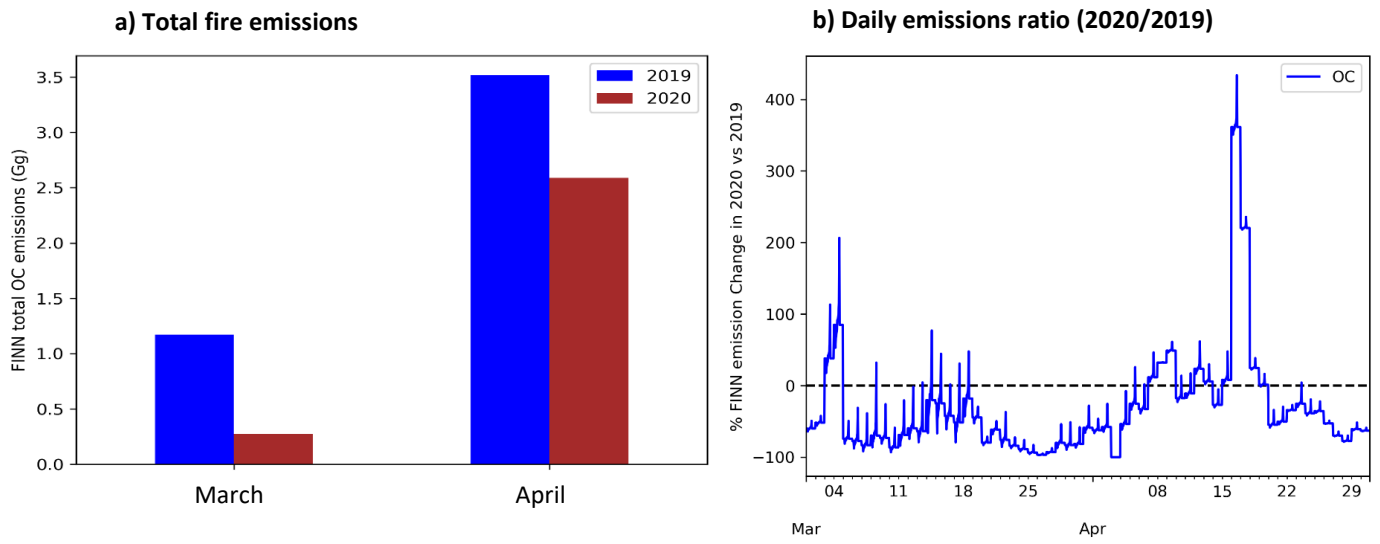


Figure S2 Comparison of FINN biomass burning emissions between 2019 and 2020 for a) total emissions and b) the ratio of daily emissions

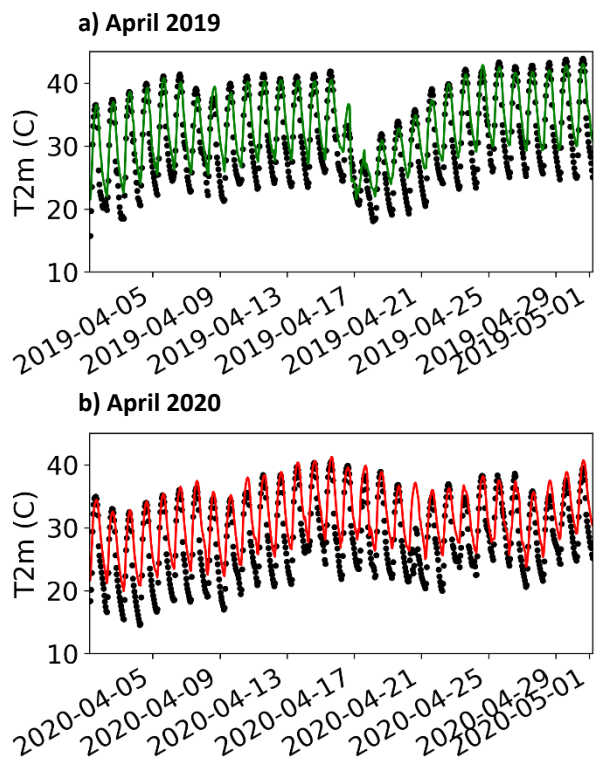


Figure S3 Timeseries of 2m temperature in model (black dots) and MERRA-2 (green line in 2019 (a) and red line in 2020 (b)) in a grid cell over Delhi (28.6N, 77.19 E)

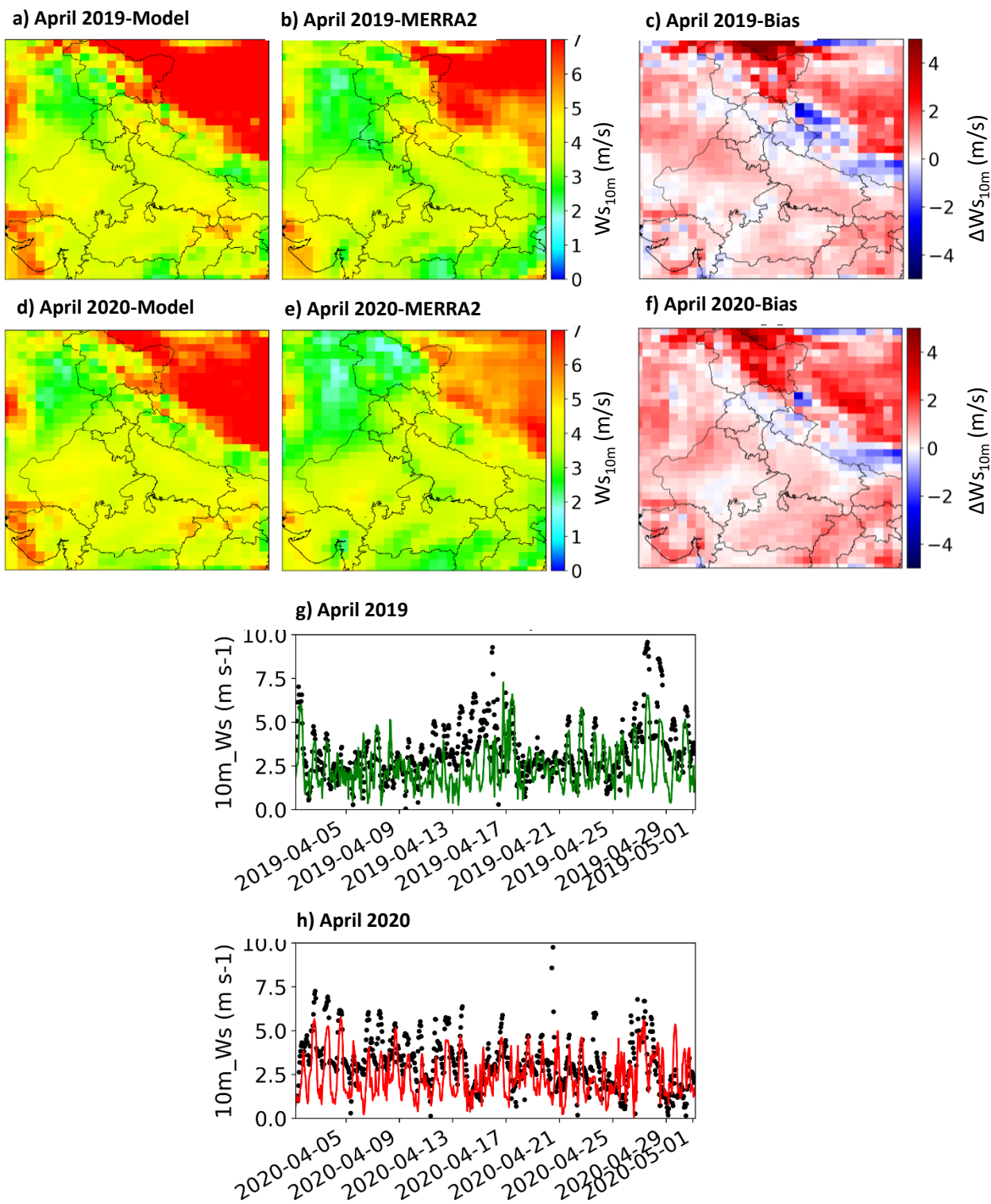


Figure S4 Temporospacial performance of the model for 10 m wind speed in April 2019 and 2020. Timeseries (g,h) are for a location in Delhi (28.6N, 77.19 E)

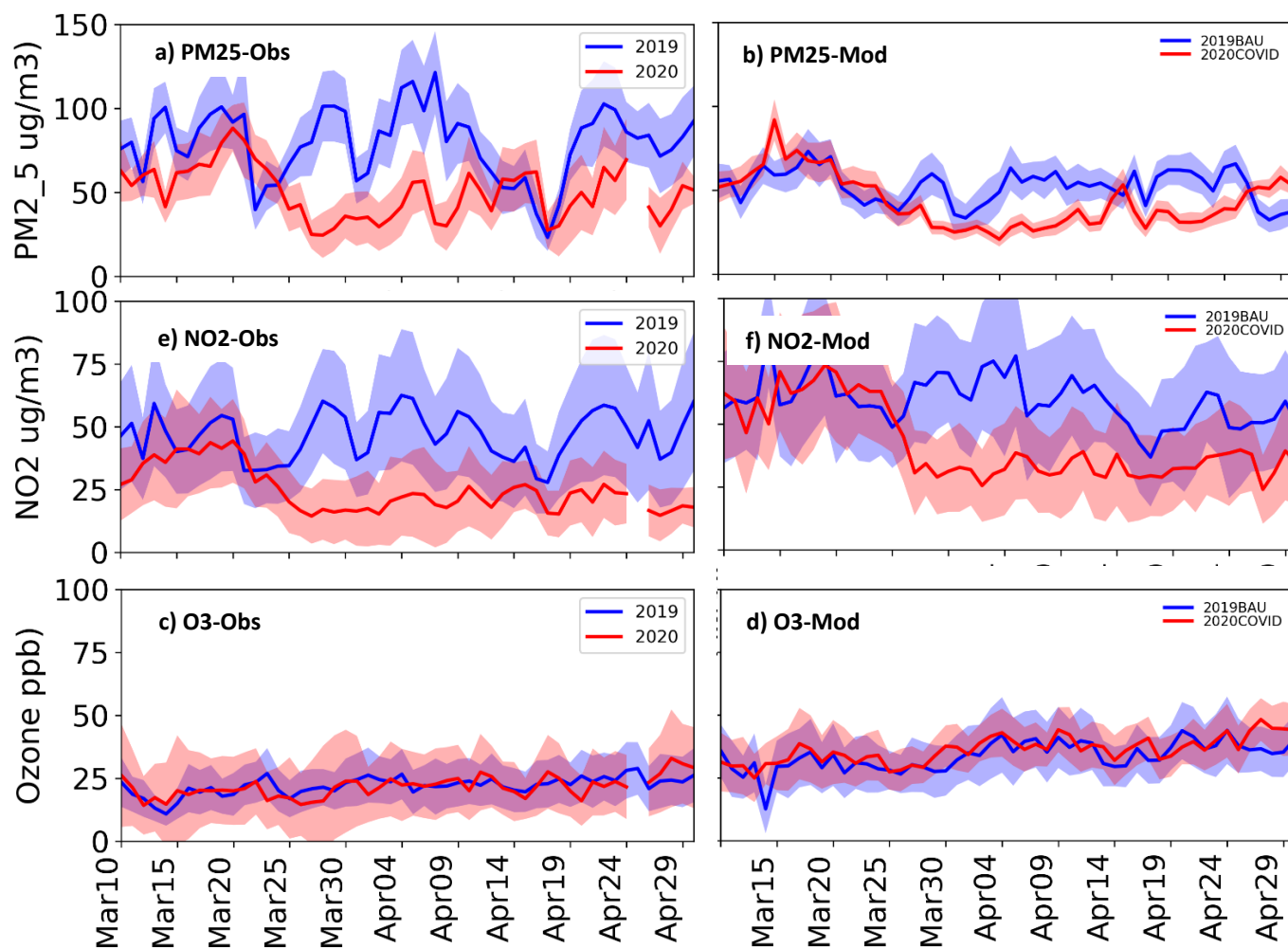


Figure S5 24-hour averaged PM_{2.5} (top row), NO₂ (middle row), and ozone (bottom row) concentrations measured over CPCB stations in Delhi (left column) and modeled over Urban region (right column) between 10 March and 30 April in 2019 (green colors) and 2020 (red colors). The shaded regions show ±1STD. The observed data were extracted from the ground measurements data in Delhi, while the modeled data were averaged in the Urban subdomain.

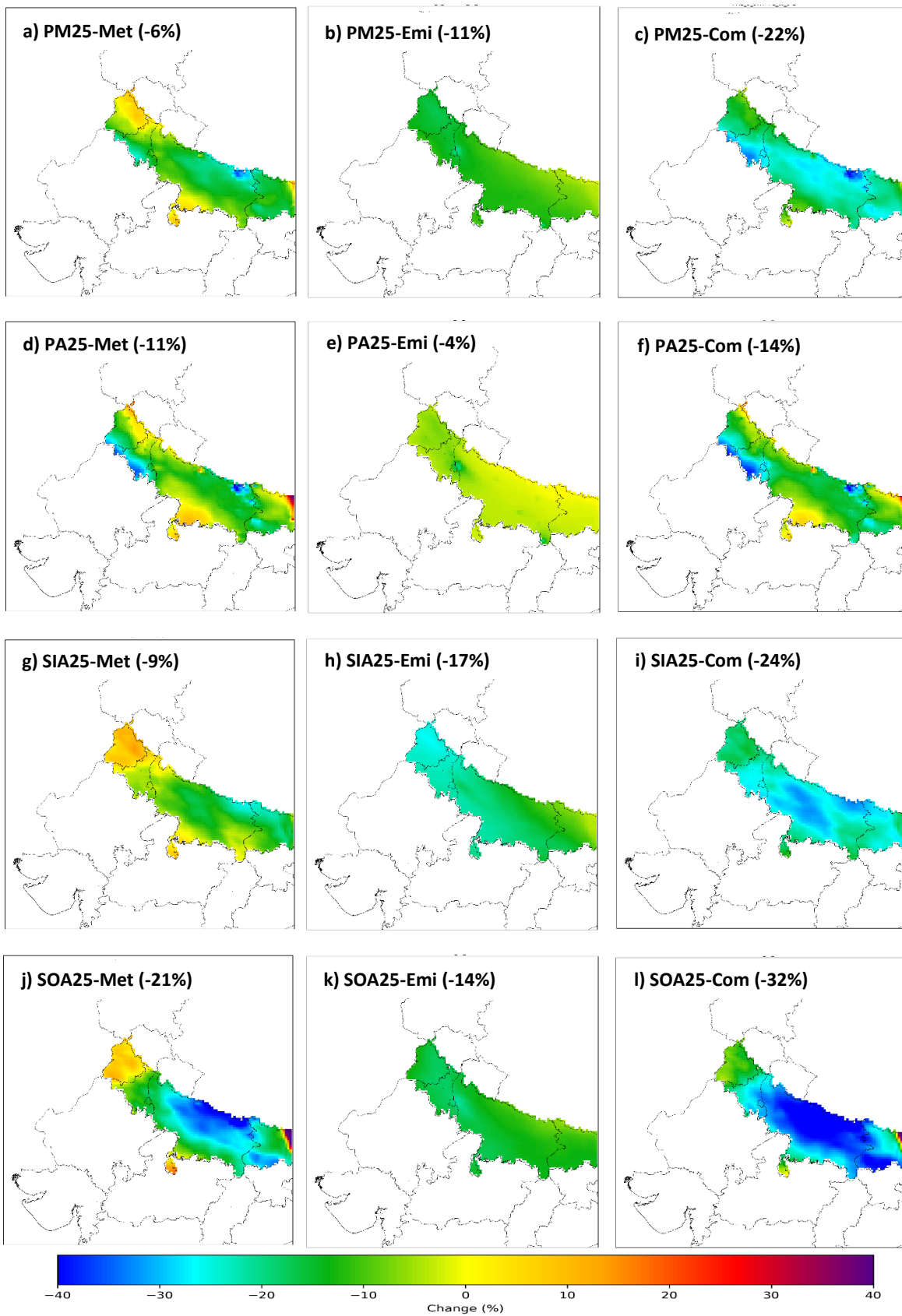


Figure S6 Responses of April averaged daytime PM_{2.5} (first row), PA_{2.5} (second row), SIA_{2.5} (third row), and SOA_{2.5} (fourth row) concentrations in the IGP to meteorology (left column), emission (middle column), and combined (right column) effects. The numbers in the parenthesis show the averaged change over the colored region between April 2020 and 2019.

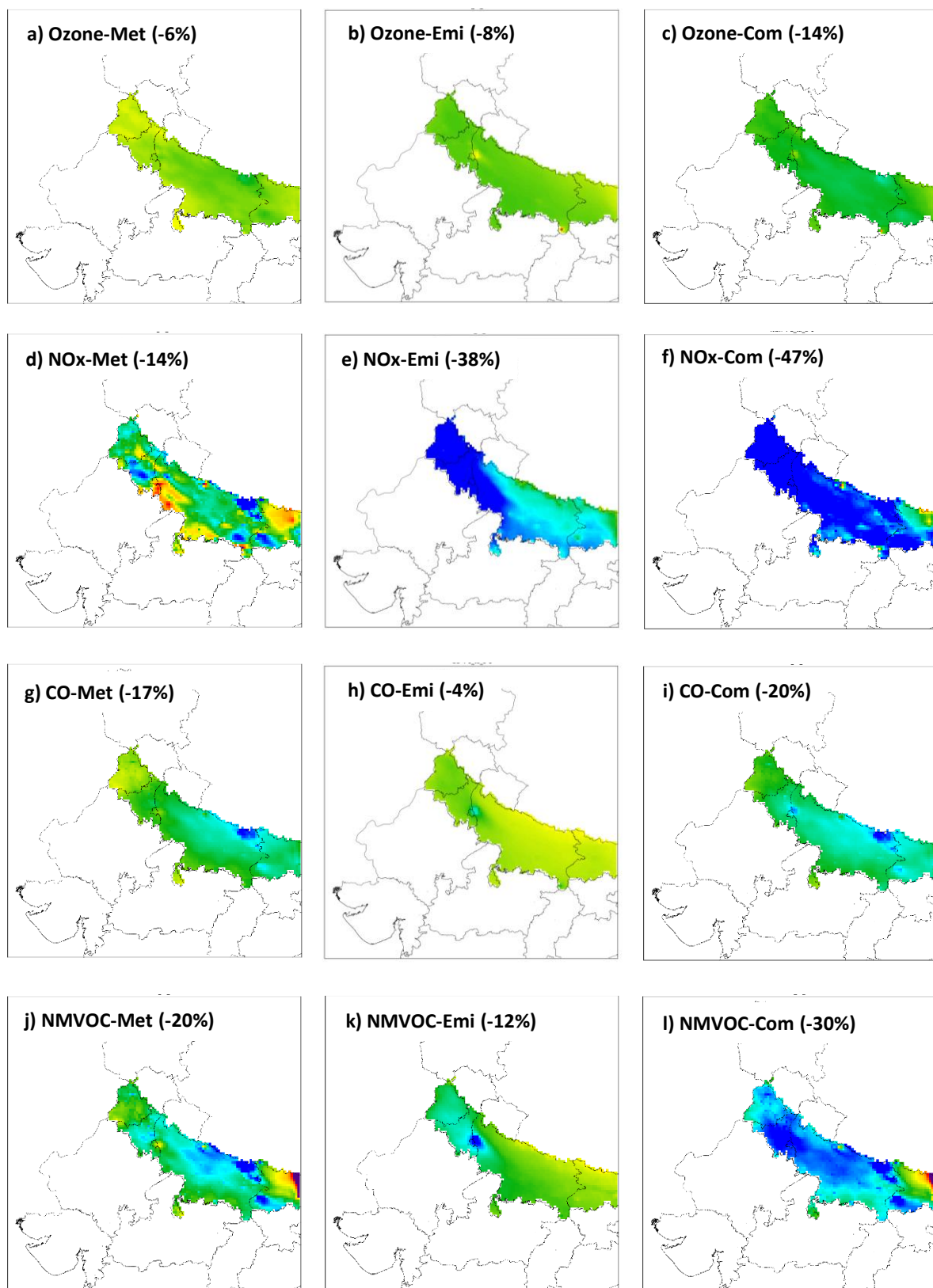
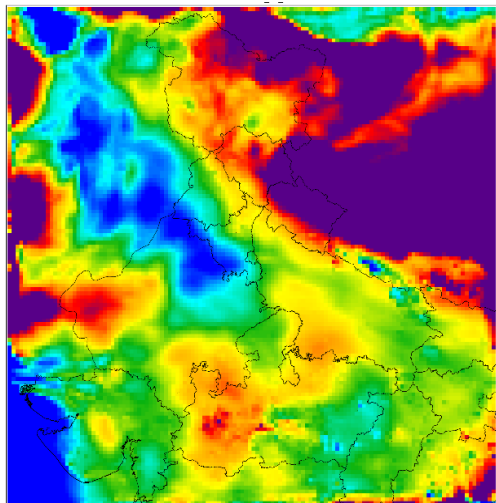
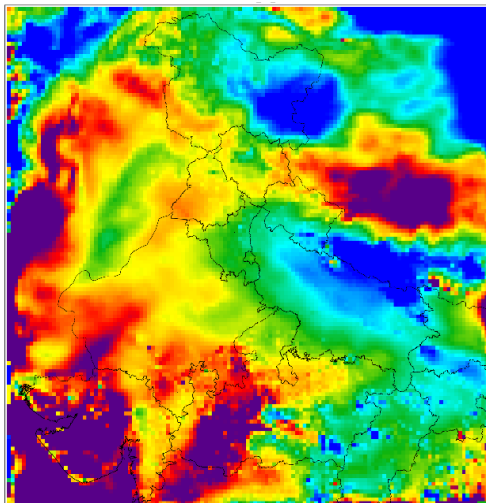


Figure S7 Responses of April averaged daytime ozone (first row), NOx (second row), CO (third row), and NMVOC (fourth row) concentrations in the IGP to meteorology (left column), emission (middle column), and combined (right column) effects. The numbers in the parenthesis show the averaged change over the colored region between April 2020 and 2019.

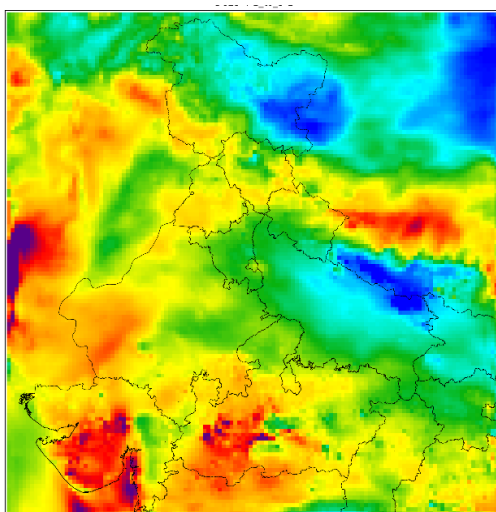
a) OIN_{2.5}-Met



b) OC_{2.5}-Met



c) BC_{2.5}-Met



d) Ws10- Met

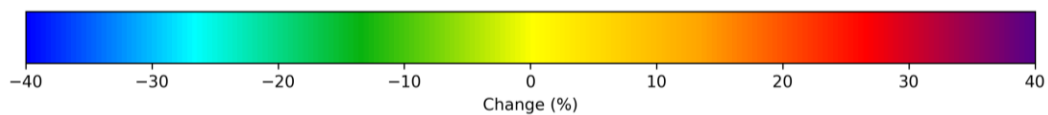
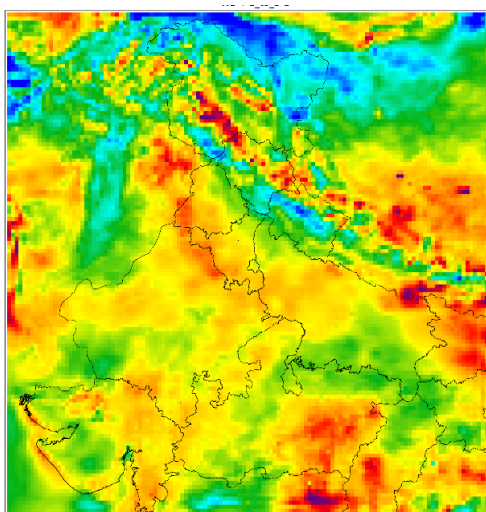


Figure S8 Responses of April averaged daytime a) other inorganics (OIN_{2.5}), b) OC_{2.5}, c) BC_{2.5}, and d) 10-m wind speed (Ws10) to meteorology effects.

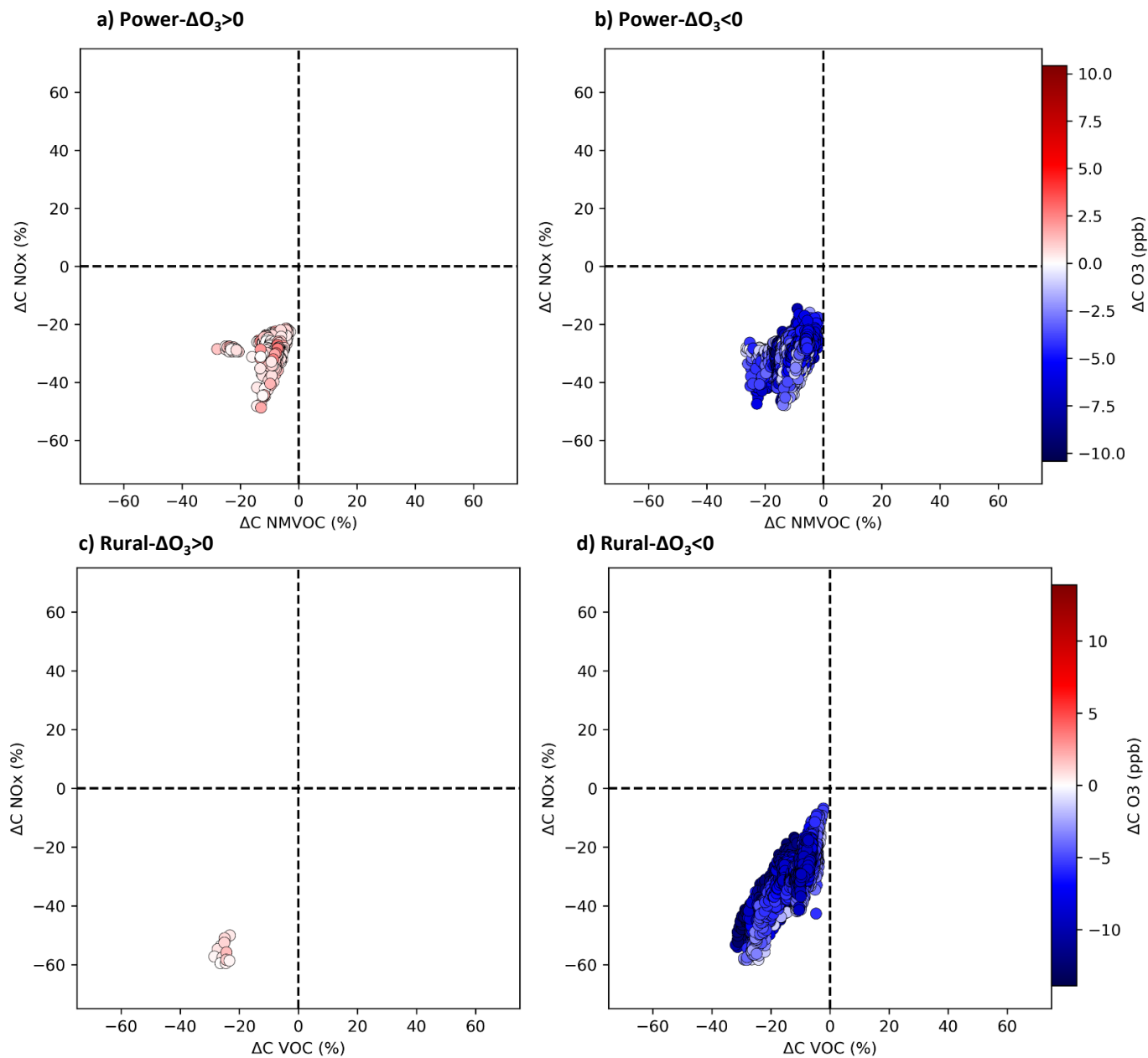


Figure S9 Plot of changes in NOx (Y-axis) and NMVOC (X-axis) concentrations due to the lockdown (2020COVID – 2020BAU) and ozone responses in all the grid cells within the Power (a, b) and Rural (c, d) regions (20 grid cells) during April (30 days) daytime (1000-1700 LT) hours (total data points are 4800). X- and Y-axis are normalized values. 5th layer in the model was selected to minimize the impacts of direct emissions.

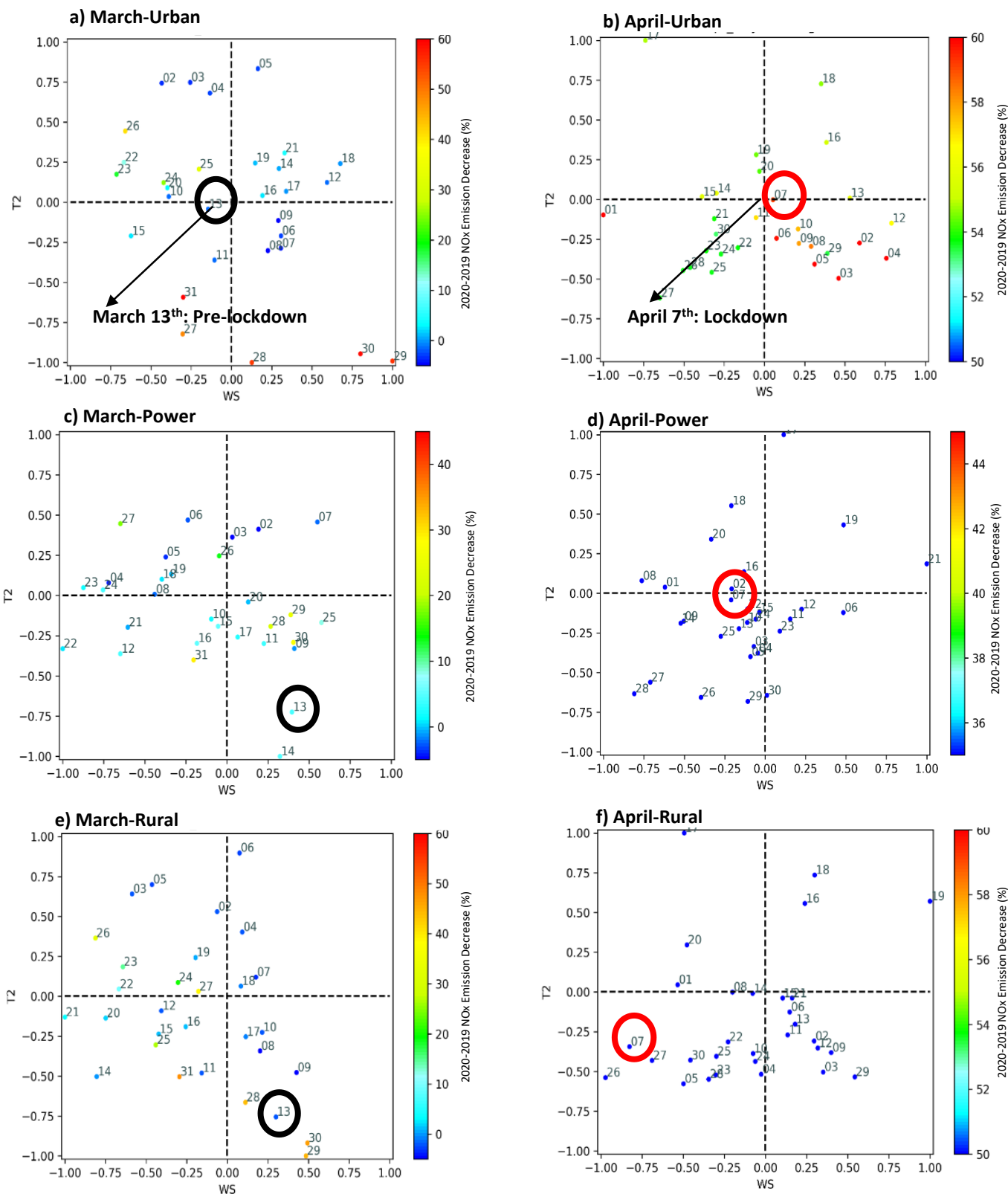


Figure S10 The changes between 2020 and 2019 in averaged daytime 2-m temperature (Y-axis) and 10-m wind speed (X-axis) in March (left column) and April (right column) in Urban (top row), Power (middle row), and Rural (bottom row). The numbers show the day of the month. The colors show the percentage of decrease in NOx emission in each day (negative value shows an increase in emission). The black (red) circle in top panel shows the day with the lowest overall changes in meteorology in March (April). X- and Y-axis are normalized changes.

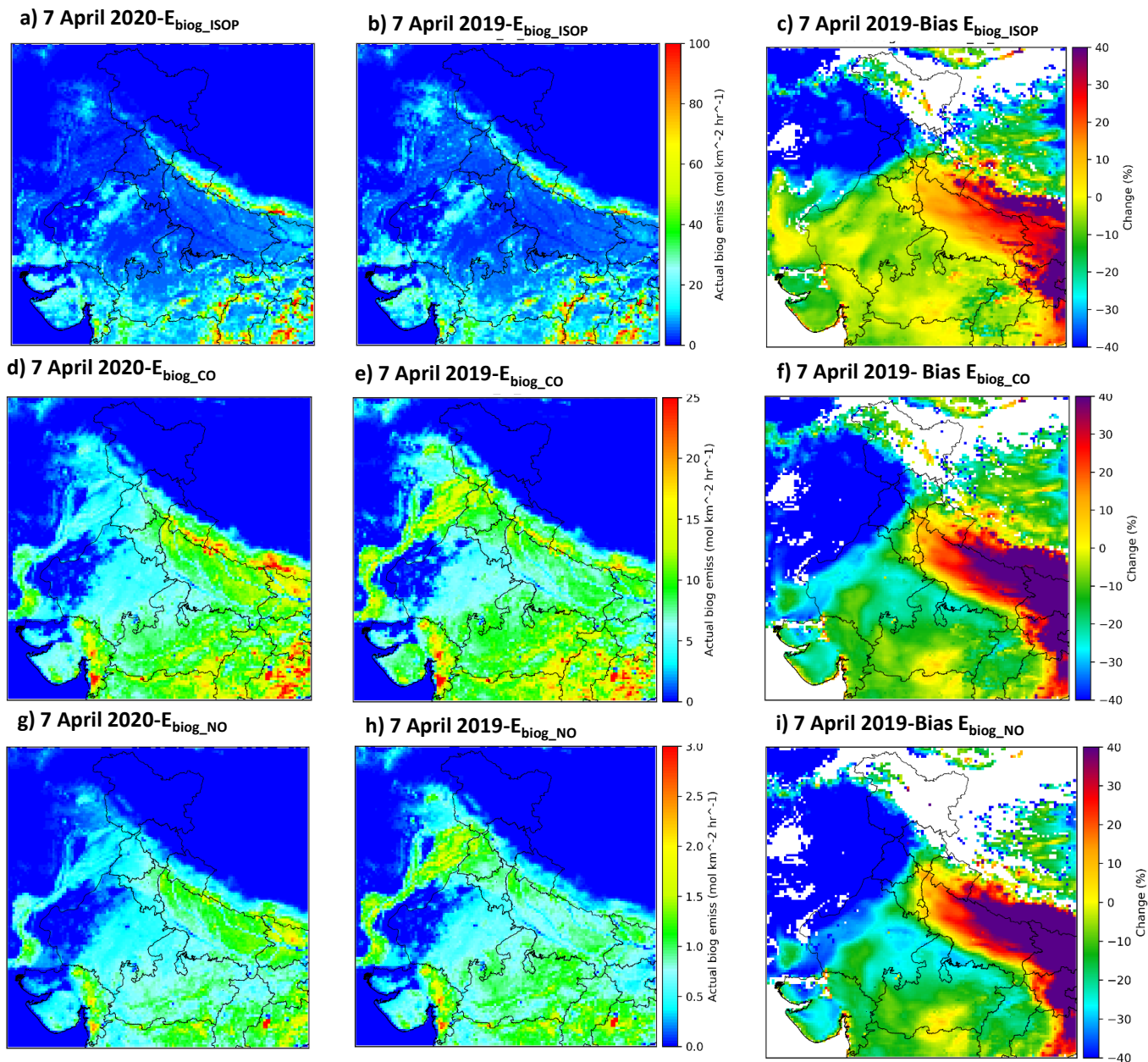


Figure S11 Biogenic emission from MEGAN in 7 April 2020 (left column) and 2019 (middle column) and their corresponding changes (right column) for isoprene (top row), CO (middle row), and NO (bottom row)

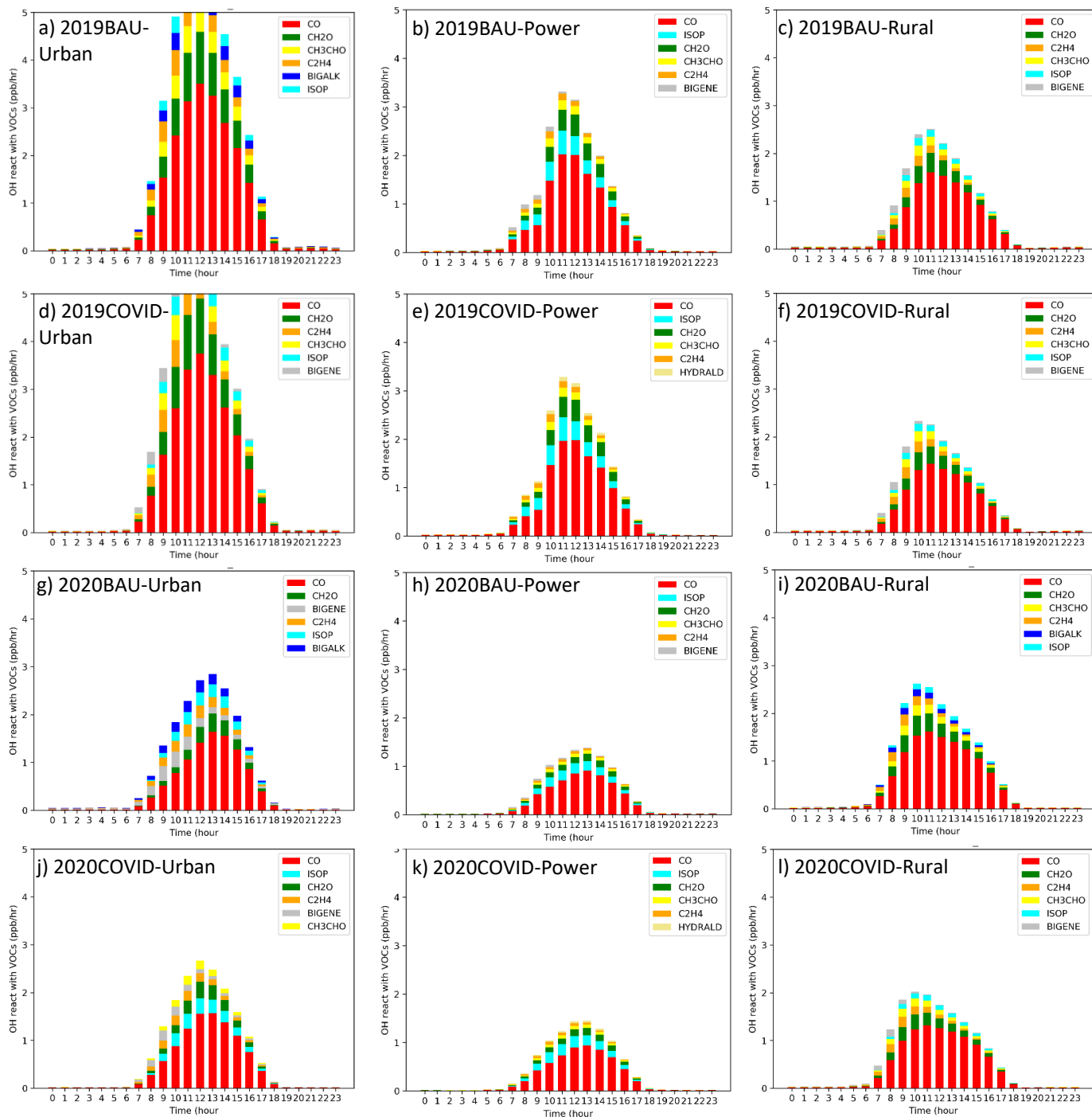


Figure S12 Diurnal cycle of OH reactivity with VOC species (averaged within the PBL) in Urban (left column), Power (middle column), and Rural (right column) for each scenario. Only the first six VOC species with higher total contribution is shown. The legend in each panel shows the ranking of the species for each scenario.

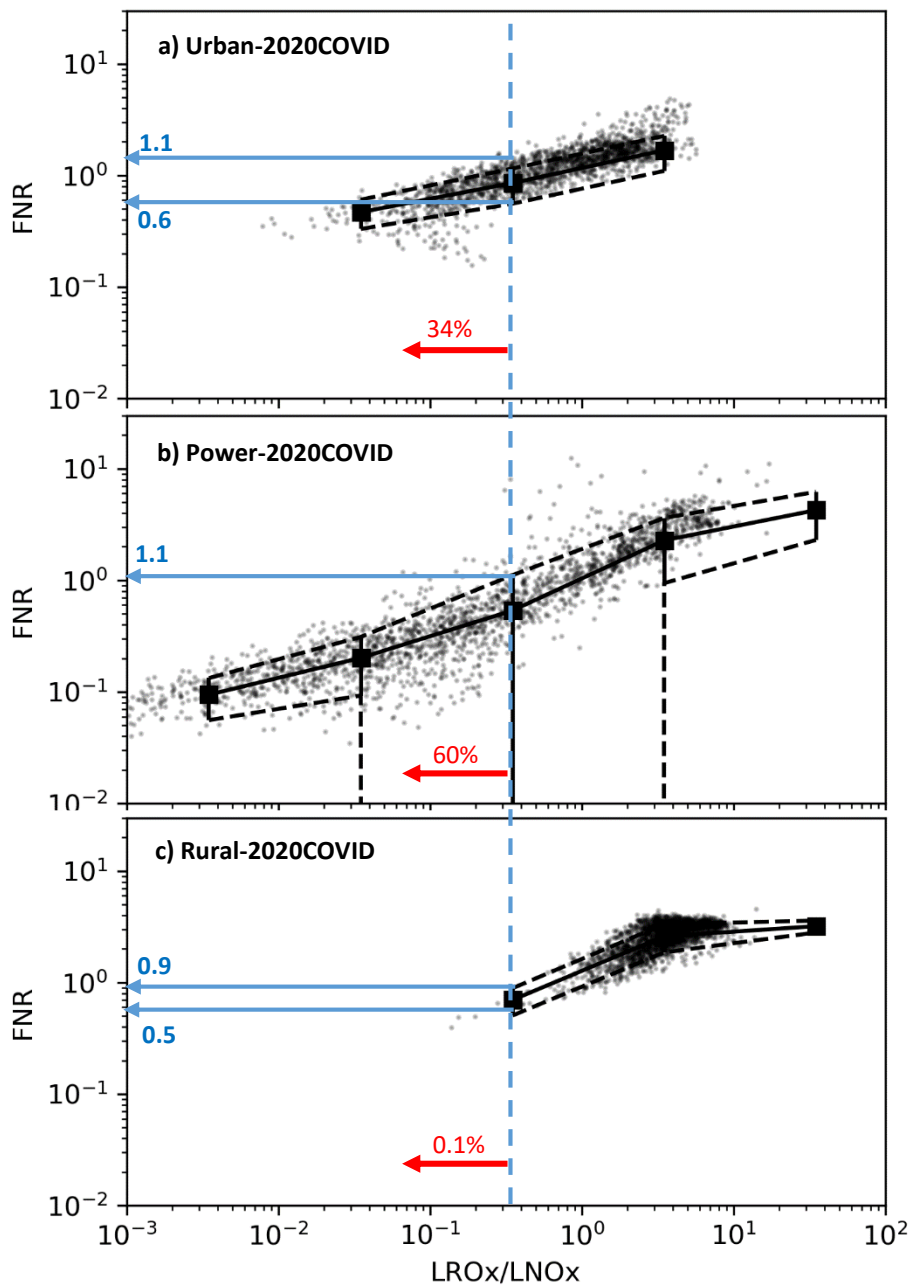


Figure S13 Plots of point-to-point FNR ratio (within the PBL) as a function of LROx/LNOx ratio during afternoon hours (1230-1430 LT) for 2020COVID scenario in a) Urban, b) Power, and c) Rural regions. Binned averages (black squares) and standard deviations (vertical black bars) were calculated. The vertical dashed blue line represents LROx/LNOx ratio of 0.35. The horizontal blue vectors show the FNR transition range in each region (numbers in blue show the values). Red values show the percentage of points in each region that fall in VOC-limited regime based on LROx/LNOx information.

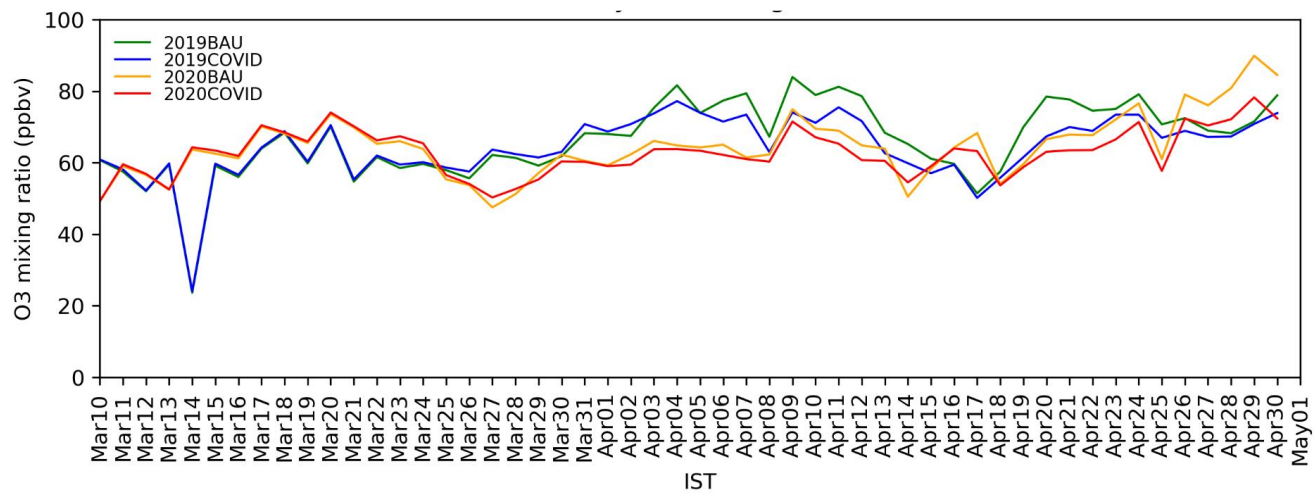


Figure S14 Daytime averaged ozone mixing ratio averaged within Urban region using all the scenarios

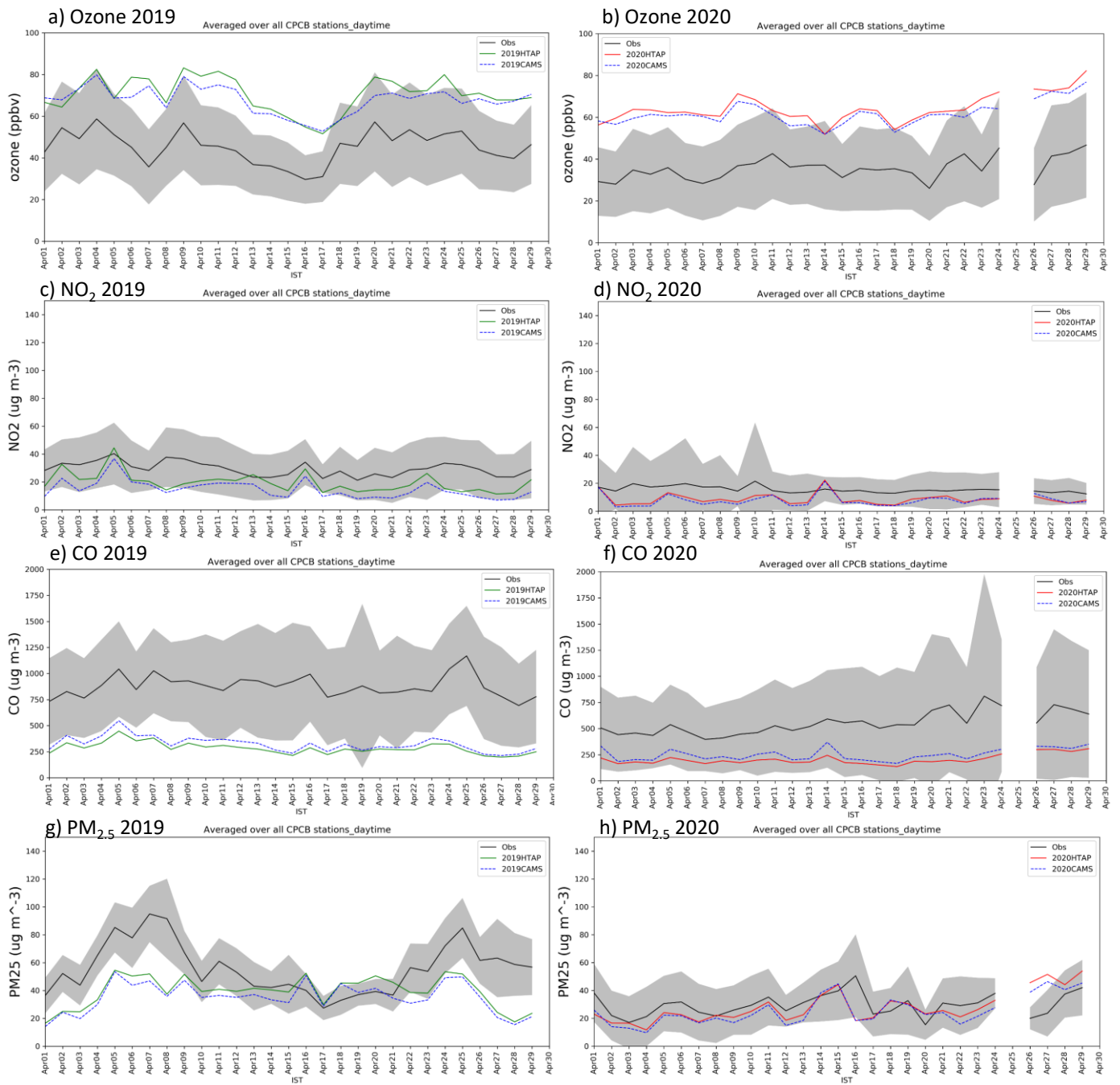


Figure S15 Simulated daytime averaged and measured data in CPCB stations in Delhi for ozone, NO₂, CO, and PM_{2.5} concentrations using HTAP and CAMS emission inventories in April 2019 (left column) and 2020 (right column). Shaded area shows 1STD of the measured values.

Table S1 The mapping between HTAP and CAMS VOC species to MOZART mechanism in WRF-Chem

MOZART	HTAP	CAMS
C2H2	ethyne	voc9
C2H4	ethene	voc7
C2H6	ethane	voc2
C3H6	propene	voc8
C3H8	propane	voc3
BIGALK	butanes + pentanes + hexanes&higher-alkanes + esters + ethers	voc4+voc5+voc6+voc18+voc19
BIGENE	other-alkenes	voc12
BENZENE	benzene	voc13
TOLUENE	toluene	voc14
XYLENES	xylene + trimethylbenzenes + other-aromatics	voc15+voc16+voc17
CH2O	methanal	voc21
CH3CHO	other-alkanals (aldehydes)	voc22
CH3OH	0.15 * alcohols	0.15*voc1
C2H5OH	0.85 * alcohols	0.85*voc1
CH3COCH3	0.2 * ketones	0.2*voc23
MEK	0.8 * ketones	0.8*voc23
HCOOH	0.5 * acids	0.5*voc24
CH3COOH	0.5 * acids	0.5*voc24
ISOP		voc10
C10H16		voc11

Table S2 Total emissions in HTAP inventory using BAU and COVID scenarios in March

Species (unit)	India		Urban		Power		Rural	
	BAU	COVID	BAU	COVID	BAU	COVID	BAU	COVID
NMVOC (Gmol)	14.23	13.8	0.45	0.4	0.03	0.03	0.04	0.04
NOx (Gmol)	9.52	8.69	0.49	0.43	0.42	0.4	0.01	0.013
CO (Gmol)	119.0	115.53	2.47	2.18	0.98	0.94	0.26	0.26
SO2 (Gmol)	7.22	6.75	0.18	0.17	0.46	0.44	0.00	0.00
BC (Tg)	45.54	45.66	0.69	0.62	0.09	0.09	0.08	0.08
OC (Tg)	106.75	111.14	0.76	0.73	0.18	0.19	0.23	0.24

Table S3 Total emissions in HTAP inventory using BAU and COVID scenarios in April

Species (unit)	India		Urban		Power		Rural	
	BAU	COVID	BAU	COVID	BAU	COVID	BAU	COVID
NMVOC (Gmol)	13.28	11.14	0.42	0.19	0.03	0.02	0.04	0.03
NO _x (Gmol)	8.82	5.21	0.46	0.2	0.38	0.29	0.01	0.007
CO (Gmol)	110.9	93.59	2.28	1.05	0.9	0.69	0.25	0.21
SO ₂ (Gmol)	6.6	4.49	0.17	0.11	0.42	0.32	0.00	0.00
BC (Tg)	42.15	41.44	0.63	0.34	0.08	0.09	0.08	0.09
OC (Tg)	99.3	114.38	0.7	0.55	0.17	0.20	0.22	0.26

Table S4 Daytime (1000-1700 LT) statistics. Mean (\pm standard deviation), Normalized Mean Bias (NMB), Root Mean Square Error (RMSE), and Pearson Correlation Coefficient averaged for all CPCB stations in Delhi in 2019 (scenario: 2019BAU) and 2020 (scenario: 2020COVID) using HTAP and CAMS anthropogenic emission inventories.

Variable	Year	OBS Mean (± 1 std)	<i>HTAP</i>				<i>CAMS</i>			
			<i>MODEL Mean</i> (± 1 std)	<i>NMB</i> (%)	<i>RMSE</i>	<i>R</i> (%)	MODEL Mean (± 1 std)	NMB (%)	RMSE	R (%)
O ₃ (ppb)	2019	50(± 11)	71(± 13)	+43	25	+37	69(± 11)	+38	22	+38
	2020	36(± 6)	64(± 9)	+78	30	+37	62(± 8)	+70	27	+36
PM _{2.5} ($\mu\text{g}/\text{m}^3$)	2019	56(± 22)	39(± 12)	-31	27	+36	34(± 12)	-39	30	+44
	2020	30(± 13)	28(± 12)	-7	14	+42	25(± 11)	-17	13	+47
NO ₂ ($\mu\text{g}/\text{m}^3$)	2019	28(± 7)	18(± 13)	-35	15	+38	13(± 11)	-55	18	+43
	2020	14(± 2)	7(± 7)	-47	9	+33	6(± 7)	-56	10	+30
CO ($\mu\text{g}/\text{m}^3$)	2019	829(± 135)	277(± 86)	-67	566	+42	305(± 109)	-63	541	+40
	2020	566(± 132)	201(± 57)	-64	382	+53	237(± 83)	-58	351	+43

Table S5 24-hour averages statistics. Mean (\pm standard deviation), Normalized Mean Bias (NMB), Root Mean Square Error (RMSE), and Pearson Correlation Coefficient averaged for all CPCB stations in Delhi in 2019 (scenario: 2019BAU) and 2020 (scenario: 2020COVID) using HTAP and CAMS anthropogenic emission inventories. 17285 and 22880 hourly points prior to applying filters were used in 2019 and 2020, respectively.

Variable	Year	OBS Mean (± 1 std)	<i>HTAP</i>				<i>CAMS</i>			
			<i>MODEL Mean</i> (± 1 std)	<i>NMB</i> (%)	<i>RMSE</i>	<i>R</i> (%)	MODEL Mean (± 1 std)	NMB (%)	RMSE	R (%)
O ₃ (ppb)	2019	27(± 20)	31(± 32)	+18	19	+87	37(± 27)	+38	17	+85
	2020	24(± 12)	35(± 25)	+47	20	+84	38(± 20)	+59	19	+82
PM _{2.5} ($\mu\text{g}/\text{m}^3$)	2019	82(± 40)	56(± 20)	-31	42	+53	59(± 26)	-28	40	+57
	2020	45(± 23)	38(± 15)	-17	21	+51	41(± 19)	-9	19	+60
NO ₂ ($\mu\text{g}/\text{m}^3$)	2019	46(± 20)	70(± 45)	+51	42	+68	56(± 40)	+22	34	+60
	2020	20(± 7)	42(± 32)	+116	36	+61	34(± 27)	+72	27	+54
CO ($\mu\text{g}/\text{m}^3$)	2019	1095(± 369)	563(± 270)	-49	622	+53	685(± 356)	-37	539	+53
	2020	670(± 179)	339(± 136)	-49	363	+58	516(± 261)	-23	266	+56

Table S6 Reactions used to calculate the LROx in IRR analysis

MOZART Reactions	IRR reactions (LROx)
ALKO2 + HO2 -> ALKOOH	ALKO2_HO2_IRR
BENZO2 + HO2 -> BENZOOH	BENZO2_HO2_IRR
BZOO + HO2 -> BZOOH	BZOO_HO2_IRR
C2H5O2 + HO2 -> C2H5OOH + O2	C2H5O2_HO2_IRR
C3H7O2 + HO2 -> C3H7OOH + O2	C3H7O2_HO2_IRR
C6H5O2 + HO2 -> C6H5OOH	C6H5O2_HO2_IRR
CH3O2 + HO2 -> CH3OOH + O2	CH3O2_HO2_IRR
HO2 + HO2 -> H2O2 + O2	HO2_HO2_H2O_IRR
HO2 + aer -> 0.5*H2O2	HO2_IRR
HOCH2OO + HO2 -> HCOOH	HOCH2OO_HO2_IRR
ISOPA02 + HO2 -> ISOPOOH	ISOPA02_HO2_IRR
MACRO2 + HO2 -> MACROOH	MACRO2_HO2_IRR
MBONO3O2 + HO2 ->	MBONO3O2_HO2_IRR
MBOO2 + HO2 -> MBOOOH	MBOO2_HO2_IRR
MEKO2 + HO2 -> MEKOOH	MEKO2_HO2_IRR
NTERPO2 + HO2 -> NTERPOOH	NTERPO2_HO2_IRR
OH + HO2 -> H2O + O2	OH_HO2_IRR
PHENO2 + HO2 -> PHENOOH	PHENO2_HO2_IRR
PO2 + HO2 -> POOH + O2	PO2_HO2_IRR
RO2 + HO2 -> ROOH	RO2_HO2_IRR
TERP2O2 + HO2 -> TERP2OOH	TERP2O2_HO2_IRR
TERPO2 + HO2 -> TERPOOH	TERPO2_HO2_IRR
TOLO2 + HO2 -> TOLOOH	TOLO2_HO2_IRR
XO2 + HO2 -> XOOH	XO2_HO2_IRR
XYLENO2 + HO2 -> XYLENOOH	XYLENO2_HO2_IRR
XYLOLO2 + HO2 -> XYLOLOOH	XYLOLO2_HO2_IRR

Table S7 Reactions used to calculate the LNOx in IRR analysis

MOZART Reactions	IRR reactions
CH3CO3 + NO2 + M -> PAN + M	CH3CO3_NO2_IRR
DICARBO2 + NO2 + M -> NDEP + M	DICARBO2_NO2_IRR
MACRO2 + NO -> .8 ONITR + nume	MACRO2_NO_a_IRR
MALO2 + NO2 + M -> NDEP + M	MALO2_NO2_IRR
MDIALO2 + NO2 + M -> NDEP + M	MDIALO2_NO2_IRR
NO2 + OH + M -> HNO3 + M	OH_NO2_IRR
PHENO + NO2 -> NDEP	PHENO_NO2_IRR

Table S8 Total OH reactivity with VOCs and NO₂ and corresponding ratio in Urban, Power, and Rural for April 7th (lockdown sample day)

Scenario	OH+VOC	OH+NO₂	(OH+VOC)/(OH+NO₂)
Urban			
2019BAU	58.67	13.75	4.27
2019COVID	54.03	8.15	6.63
2020BAU	27.3	8.2	3.3
2020COVID	23.28	4.59	5.07
Power			
2019BAU	24.23	7.65	3.17
2019COVID	23.91	6.22	3.84
2020BAU	12.21	6.63	1.84
2020COVID	12.61	5.8	2.17
Rural			
2019BAU	20.78	2.68	7.75
2019COVID	19.62	1.78	11.02
2020BAU	24.21	2.27	10.67
2020COVID	19.74	1.25	15.79

References

- Granier, C., Darras, S., van der Gon, H. D., Jana, D., Elguindi, N., Bo, G., Michael, G., Marc, G., Jalkanen, J.-P., and Kuenen, J.: The Copernicus atmosphere monitoring service global and regional emissions (April 2019 version), Copernicus Atmosphere Monitoring Service, 2019.
- Guttikunda, S. K., Nishadh, K., and Jawahar, P.: Air pollution knowledge assessments (APnA) for 20 Indian cities, *Urban Climate*, 27, 124-141, 2019.
- Jena, C., Ghude, S. D., Kumar, R., Debnath, S., Govardhan, G., Soni, V. K., Kulkarni, S. H., Beig, G., Nanjundiah, R. S., and Rajeevan, M.: Performance of high resolution (400 m) PM 2.5 forecast over Delhi, *Scientific reports*, 11, 1-9, 2021.
- Pfister, G., Wang, C. T., Barth, M., Flocke, F., Vizuete, W., and Walters, S.: Chemical Characteristics and Ozone Production in the Northern Colorado Front Range, *Journal of Geophysical Research: Atmospheres*, 124, 13397-13419, 2019.